REVIEW
SPACE PHYSICS

Earth and Planetary Physics
2: 257–275, 2018
doi: 10.26464/epp2018025

A brief review of equatorial ionization anomaly and ionospheric irregularities

Nanan Balan[1,2*], LiBo Liu[1,2,3], and HuiJun Le[1,2,3]

[1]Key Laboratory of Earth and Planetary Physics, Institute of Geology and Geophysics, Chinese Academy of Sciences, Beijing 100029, China;

[2]Institutions of Earth Science, Chinese Academy of Sciences, Beijing 100029, China;

[3]College of Earth and Planetary Sciences, University of the Chinese Academy of Sciences, Beijing 100049, China

Abstract: Following a brief history and progress of ionospheric research, this paper presents a brief review of the recent developments in the understanding of two major phenomena in low and mid latitude ionosphere—the equatorial ionization anomaly (EIA) and involved equatorial plasma fountain (EPF) and ionospheric irregularities. Unlike the easy-to-understand misinterpretations, the EPF involves field perpendicular $\boldsymbol{E}\times\boldsymbol{B}$ plasma drift and field-aligned plasma diffusion acting together and plasma flowing in the direction of the resultant at all points along the field lines at all altitudes. The EIA is formed mainly from the removal of plasma from around the equator by the upward $\boldsymbol{E}\times\boldsymbol{B}$ drift creating the trough and consequently the crests with small accumulation of plasma at the crests when the crests are within ~±20° magnetic latitudes and no accumulation when they are beyond ~±25° magnetic latitudes. The strong EIA under magnetically active conditions arises from the simultaneous impulsive action of eastward prompt penetration electric field and equatorward neutral wind. Intense ionospheric irregularities develop in the post-sunset bottom-side equatorial ionosphere when it rises to high altitudes, and evolve nonlinearly into the topside. Pre-reversal enhancement (PRE) of the vertical upward $\boldsymbol{E}\times\boldsymbol{B}$ drift and its fluctuations amplified during PRE provide the driving force and seed, with neutral wind and gravity waves being the primary sources. At low solar activity especially in summer when fast varying PRE is absent, the slow varying gravity waves including large scale waves (LSW) seem to act as both driver and seed for weak irregularities. At mid latitudes, the irregularities are weak and associated with medium scale traveling ionospheric disturbances (MSTIDs). A low latitude minimum in the occurrence of the irregularities at March equinox predicted by theoretical models is identified. The minimum occurs on the poleward side of the EIA crest and shifts equatorward from ~25° magnetic latitudes at high solar activity to below 17° at low solar activity.

Keywords: equatorial ionization anomaly; ionospheric irregularities

Citation: Balan N., Liu L. B., and Le H. J. (2018). A brief review of equatorial ionization anomaly and ionospheric irregularities. *Earth Planet. Phys.*, *2*(4), 257–275. http://doi.org/10.26464/epp2018025

1. Introduction

As early as 1839 Gauss postulated an electrically conducting region of the atmosphere to explain the observed daily variation of Earth's magnetic field (Graham, 1724–1725). On 12 December 1901, Guglielmo Marconi a challenging engineer and his assistants successfully transmitted a wireless message (three bits Morse code, three dots, for the letter S) from Cornwall in England to Newfoundland (now) in Canada costing 200,000 British pounds (Marconi's interview in 1933, Beynon, 1975). They used a spark-gap transmitter to produce a signal of frequency ~500 KHz with a power 100 times more than any radio signal previously produced, and a 152.4 m (500 feet) antenna for reception. This electronic bridging of the Atlantic Ocean was the beginning of long distance wireless communication for which Marconi got Nobel Prize in 1909. Then, the question, how Marconi's radio signal found its way around the curvature of the Earth (or why it was not lost into space) was the beginning of ionospheric research.

Soon scientists, notably Kennelly (1902) and Heaviside (1902), postulated the existence of an *ionized upper region* in the atmosphere that reflected the radio waves. Taylor (1902–1903) was among the first scientists to suggest that the ionized layer was produced by solar radiation. Twenty-three years later on the same day 12 December in 1924, Appleton and Barnett (1925) proved the existence of the ionized layer and found its height (~100 km) by comparing the phase of two signals from a BBC transmitter, one ground wave and the other reflected from the ionosphere. Appleton got Nobel Prize in 1947 for his contributions to ionospheric research. Breit and Tuve (1925) used a pulse technique (forerunner of ionosonde) to measure the heights and critical frequency of a few ionized regions.

The term *Ionosphere* was coined in 1926 by Watson-Watt. The ionized regions were named E and F regions, leaving room to discover more regions below and above. The letter E was adopted from the symbol *E* used for the electric field of the signal reflected from the lower region and consequently the letter F was used for the

Correspondence to: N. Balan, balan.nanan@yahoo.com
Received 27 JUN 2018; Accepted 12 JUL 2018.
Accepted article online 20 JUL 2018.

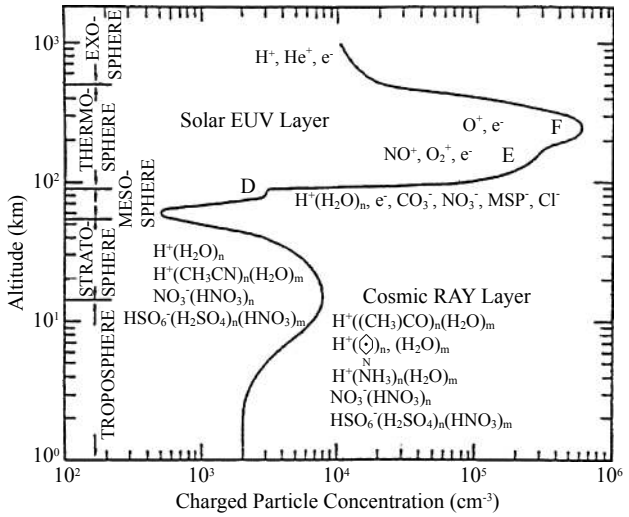

Figure 1. Typical ionization density profile; major ion species at different altitude levels are listed (from Viggiano and Arnold, 1995).

upper region. Later a D region and an occasionally occurring weak C region were detected. The F region was also found to split into F_1 and F_2 layers during daytime. More recently, a cosmic ray layer populated mainly by hydrated ions was also detected well below the main ionosphere (Figure 1).

The ionosphere is the ionized part of the upper atmosphere and neutral part is the thermosphere. The ionization is so weak that even at the peak of the ionosphere, the ion to neutral particle ratio is only up to 1:500. On a global scale, the ionosphere attains maximum height (up to ~600 km) at the magnetic equator slightly after sunset and maximum density (~3×10^6 cm^{-3}) at ~±16° magnetic latitudes just after local noon (13–14 LT). The ionosphere is produced by the ionization of neutral atmosphere (mainly atomic oxygen) with energy for the ionization coming from the sun. The movement of ionosphere is driven by neutral wind and controlled by geomagnetic field.

For practical reasons, the ionosphere can be defined as the part of the upper atmosphere where ions and electrons are present in sufficient numbers to *influence* the propagation of radio waves (Ratcliffe, 1972). The influence has both advantages and disadvantages. (1) It is mainly to exploit the advantages in HF communication and find remedies for the disadvantage in satellite-ground communication that we started studying the ionosphere. (2) Ionosphere is also studied for its disadvantages in radio astronomy. (3) The ionosphere is a natural plasma laboratory which can be studied at our will and wish, and the information gained can be used for understanding the behavior of man-made laboratory plasmas, for example, in fusion reactors. (4) The ionosphere has been studied around the world for over a century for its science.

The basic science has been understood thanks to the excellent works of a number of scientists. Chapman (1931) presented a theory for the formation of the ionosphere. His contributions are recognized through an international conference in his name. The studies should be continued for (a) understanding many special phenomena that exist in the ionosphere, (b) its interaction with the neutral atmosphere below and fully ionized magnetosphere and solar wind above, (c) its strengthening and weakening during solar storms, (d) impulsive intensification of ionospheric currents during extreme solar storms leading to severe space weather that cause extensive social and economic disturbances in the High-Tec society by damaging utility systems such as electric power grids, communication cables, oil and gas metal pipe lines, and (e) searching for possible ionospheric precursor of earthquakes.

Since its discovery, for about 60 years when ionosonde was the main instrument, the interest was mainly to compare measured electron density and height variations with theoretical predictions. With the introduction of radars, rockets and satellites measurement of electric field became easy. So there was a natural tendency to associate ionospheric variations with electric field ignoring neutral wind. The importance of neutral wind (e.g., Rishbeth, 1971) is such that the neutral atmosphere from which the ionosphere is produced moves horizontally with a velocity $\boldsymbol{U}$. The component of $\boldsymbol{U}$ parallel to the geomagnetic field lines moves the ionospheric plasma along the field lines and hence can redistribute it in latitude and height. It is also the perpendicular component of $\boldsymbol{U}$ that produces the ionospheric electric field $\boldsymbol{E}$ through the dynamo action ($\boldsymbol{E}=\boldsymbol{U}\times\boldsymbol{B}$). Though neutral wind is the primary driver of ionospheric motion, its importance was ignored for lack of data. With the advent of new techniques involving airglow (e.g., SOFDI), radars, and satellites (e.g., C/NOFS), the wind velocity has been measured in recent times. The further progress of ionospheric research will involve winds and waves from lower atmosphere, solar storms and earthquakes.

As mentioned above, many special phenomena have been discovered in the ionosphere mainly at low latitudes due to the horizontal orientation of geomagnetic field at the equator. The special phenomena include the equatorial electrojet (e.g., Egedal, 1947), equatorial plasma fountain (Hanson and Moffett, 1966), equatorial ionization anomaly (Appleton, 1946), equatorial plasma temperature anomaly (Oyama et al., 1997), equatorial temperature and wind anomaly (Raghawarao et al., 1991), spread F and plasma bubbles (Booker and Wells, 1938; Woodman and La Hoz, 1976) and F_3 layer (Balan et al., 1998). The purpose of this paper is to present a brief review of the recent developments in the understanding of two major phenomena at low and mid latitudes—the equatorial ionization anomaly and ionospheirc irregularities. The two phenomena are reviewed in Sections 2 and 3 with introductions at the beginning.

2. Equatorial Ionization Anomaly

2.1 Introduction

Because the Sun shines over the equator, the ionospheric density was expected to vary from a maximum at the equator to a minimum at high latitudes. But when the density variation was measured (Namba and Maeda; 1939; Appleton, 1946) it was found to exhibit an unexpected large structure with a trough around the equator, crests near ±15° magnetic latitudes and crest-to-trough ratio about 1.6 in daytime peak electron density (N_{max}). This large structure known as the equatorial ionization anomaly (EIA) develops in the morning at around 10 LT, continues to exist well beyond sunset and covers about half the global area in 24 hours; and

the position of the crests and crest-to-trough ratio vary with various geophysical conditions.

Following the discovery, several theories like the diffusion theory (Mitra, 1946) and electrodynamic drift theory (Martyn, 1955) were suggested to explain the anomaly (EIA). According to the diffusion theory, plasma diffuses along the geomagnetic field lines from the (otherwise) high density region at the equator to low density region at higher latitudes under the influence of gravity and pressure gradient forces, which was suggested to produce the anomaly. Martyn (1955) proposed that, in addition to diffusion, upward $\boldsymbol{E}\times\boldsymbol{B}$ drift of plasma should also be important in causing the anomaly. Later when computers became powerful enough, Rishbeth et al. (1963) showed that diffusion is important but not sufficient. The combination of the drift and diffusion theories which generate the equatorial plasma fountain (EPF), on the other hand, was successful in explaining the observations (Moffett and Hanson, 1965). Hanson and Moffett (1966) presented the first pictures of EPF and EIA in the northern hemisphere from steady state model calculations using assumed $\boldsymbol{E}\times\boldsymbol{B}$ drift velocity (the drift velocity had yet to be measured). Anderson (1973) showed the neutral wind modulation of EIA.

The Sheffield University Plasmasphere Ionosphere Model (SUPIM) (Bailey and Balan, 1996) that incorporates measured values of $\boldsymbol{E}\times\boldsymbol{B}$ drift velocity (Fejer et al., 1991) and neutral wind velocity (from horizontal wind model HWM) (Hedin et al., 1996) showed detailed pictures of the plasma fountain with and without neutral wind and their effects in producing and modulating EIA (Balan and Bailey, 1995; Balan et al., 1997). SUPIM also showed the impulsive strengthening of the fountain during the pre-reversal enhancement (PRE) of the upward $\boldsymbol{E}\times\boldsymbol{B}$ drift and reverse plasma fountain during the following downward drift. There are a number of other physics based models (not referred due to page limitation), which have also reproduced the EIA. Review articles on EIA were presented by Rajaram (1977), Moffett (1979), Stening (1992) and Balan et al. (2018).

During the early stages of major geomagnetic storms especially super storms, the daytime plasma fountain becomes a super fountain (Balan et al., 2009) and the EIA becomes strong with over 1000% increase in density at the crests that shift up to ±30° latitudes (e.g., Mannucci et al., 2005; Balan et al., 2011). Such strong EIA was suggested to occur due to strong eastward prompt penetration electric field PPEF (Kelley et al., 2004), though modeling studies later showed that the PPEF alone is unlikely to produce the strong EIA (Balan et al., 2009). The strong EIA was explained in terms of the combined effects of strong eastward PPEF and fast storm-time equatorward winds (e.g., Lin et al., 2005; Balan et al., 2010, 2011; Lu et al., 2012).

As described, theoretical models have quite successfully reproduced the observed EIA and its variations under quiet and active conditions. However, easy-to-understand misinterpretations of EPF and EIA have caused misunderstandings which have led unlikely mechanisms to be proposed for the strong EIA under active conditions. The development of EIA in the morning by ~10:30 LT, though $\boldsymbol{E}\times\boldsymbol{B}$ drift turns upward at ~06:30 LT, also has indirectly supported the misinterpretations. This part of the brief review is intended to clarify the misinterpretations using SUPIM.

SUPIM (Bailey and Balan, 1996) solves the coupled time-dependent equations of continuity, momentum and energy for the electrons and ions (O^+, H^+, He^+, N_2^+, NO^+ and O_2^+) along closed eccentric-dipole geomagnetic field lines. Recently, the N^+ ion has also been included and the lower altitude boundary is extended down from 110 km to 80 km (Souza et al., 2013). The model inputs are the measured $\boldsymbol{E}\times\boldsymbol{B}$ drift velocity (Fejer et al., 1991), neutral wind velocities from HWM93 (Hedin et al., 1996) and neutral densities from NRLMSISE (Picone et al., 2002). HWM and NRLMSISE give the wind velocities and densities as function of altitude, latitude, local time, season, and level of solar and magnetic activities. The $\boldsymbol{E}\times\boldsymbol{B}$ drift velocities used for quiet conditions are measured at the equatorial station Jicamarca and low latitude station Arecibo (Fejer et al., 1991). These drifts and zero drift are applied at apex altitudes of 90–700 km and 1500–5000 km and above 55000 km, with interpolations for the apex altitudes in between. The apex interval varies with apex as 2.5 km for 90–120 km, 5 km for 125–300 km, 10 km for 310–500 km and 20 km for 520–1000 km; and above1000 km the apex varies at intervals corresponding to 1° latitudes. The shorter intervals at lower apex are meant for conductivity calculations. The drift velocity varies with altitude and latitude according to the field line geometry.

2.2 EIA under Quiet Conditions

Though diffusion of plasma from the equator to higher latitudes was suggested to explain EIA (Mitra, 1946), it alone was found insufficient (Rishbeth et al., 1963) as illustrated in Figure 2 which shows the electron density N_e (in units of 10^5 cm^{-3}) variation obtained from the model calculations carried out with no $\boldsymbol{E}\times\boldsymbol{B}$ drift. Diffusion alone produces only a weak anomaly in the morning with crests at around ±10° magnetic latitudes (Figure 2a) due to the large plasma pressure gradient between the equator and higher latitudes, and the anomaly becomes weaker with time and disappears before noon when the pressure gradient is small. The N_e variation at noon (13 LT, Figure 2b) is centred at the equator at ~330 km height with a density of ~19 units. The density in the northern (winter) hemisphere is slightly greater than that in the southern hemisphere due to winter anomaly or larger O/N_2 ratio in winter (Liu et al., 2010). The modelling day 30 October is the beginning of winter in the north. It may be noted that the density at the latitudes (~±15°) of the crests is ~17 units.

As mentioned above, the equatorial plasma fountain (EPF) has often been viewed as vertically upward $\boldsymbol{E}\times\boldsymbol{B}$ plasma drift at the equator followed by downward diffusion (e.g., Balan et al., 1995; Lu et al., 2012; Chen et al., 2016). This easy-to-understand picture has two incorrect interpretations: (1) the drift is interpreted to act only at the equator and (2) diffusion is interpreted to follow the drift. In reality and in models, the field perpendicular $\boldsymbol{E}\times\boldsymbol{B}$ plasma drift and field-aligned plasma diffusion present all along the field lines at all altitudes act together, and plasma flows in the direction of the resultant. The fountain can rise up to ~1000 km in height over the equator and cover up to ~±30° in latitudes (at 300 km) at high solar activity (Balan et al., 1997). The altitude-latitude coverage varies with time of the day, season and level of solar activity, and has large day-to-day variability mainly due to the variability of the $\boldsymbol{E}\times\boldsymbol{B}$ drift.

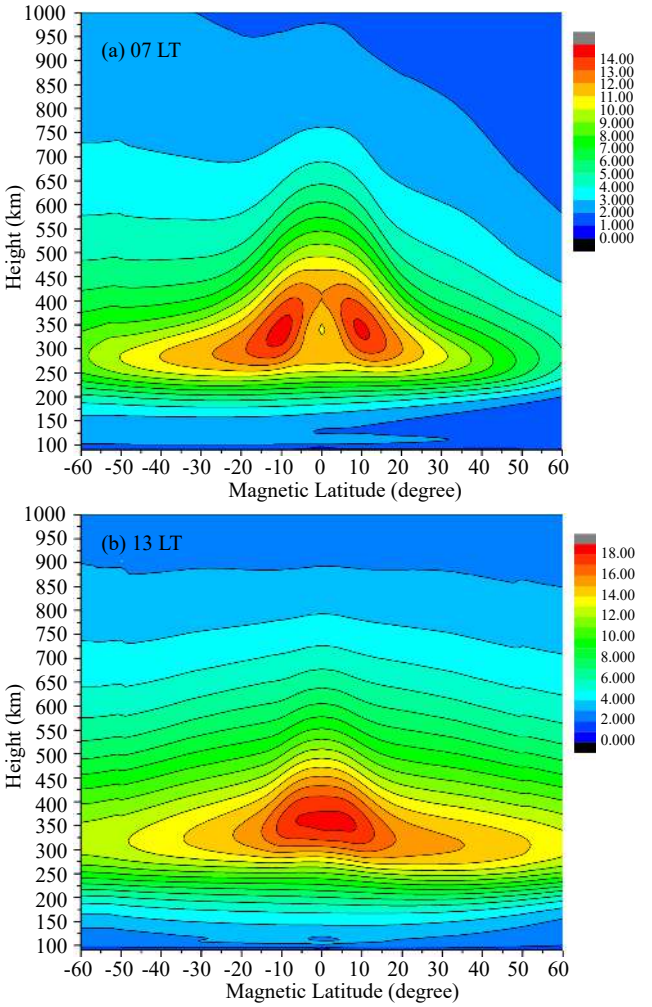

Figure 2. Altitude-latitude map of electron density N_e at (a) 07:00 LT and (b) 13:00 LT modelled by SUPIM for magnetically quiet (Ap = 4) conditions at high solar activity (day 303, $F_{10.7}$ = 268) in Jicamarca longitude (283°E) with no $\boldsymbol{E}\times\boldsymbol{B}$ drift and no neutral wind. Unit of N_e is 10^5 cm^{-3}. Positive latitude is north.

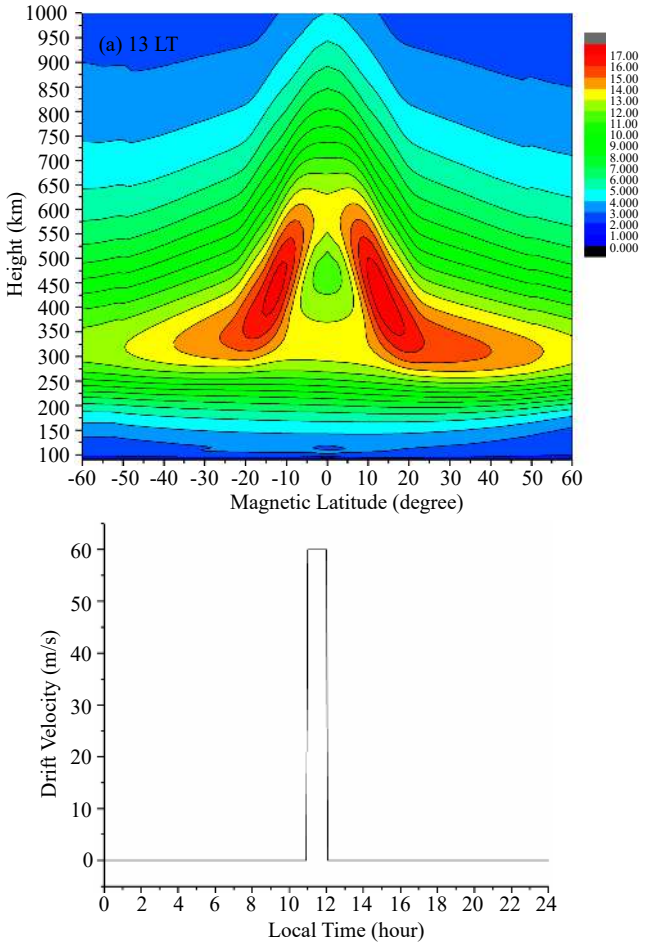

Figure 3. (a) Altitude-latitude map of N_e (Unit of N_e is 10^5 cm^{-3}) at 13:00 LT modelled by SUPIM for magnetically quiet (Ap = 4) conditions at high solar activity (day 303, $F_{10.7}$ = 268) in Jicamarca longitude (283°E) using (b) $\boldsymbol{E}\times\boldsymbol{B}$ drift used only around noon and no neutral wind. Positive latitude is north.

The EIA crests have often been viewed as forming from the accumulation of the downward diffusing plasma (e.g., Kelley et al., 2004; Lu et al., 2012). This also is not true because how could downward diffusing plasma accumulate at high altitude-latitude locations (~300 km at ±16° latitudes) where field lines are inclined, or what stops the downward diffusion at these locations against gravity. In fact, even in this scenario, plasma diffuses to the top of the crests and at the same time, as plasma pressure increases at the crests, it also diffuses down from the bottom of the crests to lower altitudes where it gets lost by chemical recombination. In reality and in models, the EIA is formed mainly from the removal of plasma from around the equator by the upward $\boldsymbol{E}\times\boldsymbol{B}$ drift creating the trough and consequently the crests with small accumulation at the crests as long as the crests are at lower latitudes. The amount of accumulation reduces as the crests shift to higher latitudes where field lines become more and more inclined and accumulation becomes zero when the crests are beyond ±25° latitudes (Balan et al., 2009).

The process of formation of the EIA can be illustrated by comparing Figures 2 and 3. Figure 3a is obtained from the model calculations carried out for the same conditions as for Figure 2 but using an assumed upward $\boldsymbol{E}\times\boldsymbol{B}$ drift (Figure 3b) applied for an hour just before noon (11:00–12:00 LT) and no drift at other local times. The drift is applied only just before noon so that the EIA formation (around noon of photo-chemical equilibrium) is not dominated either by production or chemical loss of ionization. The N_e variation at 13:00 LT (Figure 3a) exhibits well developed (nearly) symmetric EIA with crests at ~±15° latitudes at ~400 km height; density at the crests is ~18 units and crest-to-tough ratio is ~1.5. Compared to the N_e variation with no EIA (Figure 2b), the density at the trough of EIA is reduced by ~40% (from 19 units to 12 units) while the density at the crests (18 units, Figure 3a) is nearly equal to the density (17 units) at the same location (~±15°) but with no EIA (Figure 2b). This clearly indicates that the EIA crests are formed mainly by the removal of plasma from around the equator creating the trough with very small accumulation at the crests.

However, the density in the topside ionosphere around the equator (~±10°) with drift (Figure 3a) is greater than that without the drift (Figure 2a) due to the (nearly) horizontal field lines support-

ing the upward drifted plasma. This results in smaller trough-to-crest ratio in TEC than N_{max} (Balan and Bailey, 1995). Figure 2a also shows clear F_3 layer developed around the equator.

The model results also show well-developed EIA shortly after the application of the drift (Figure 3a), within about an hour in this case. However, observations (and modelling using measured $\boldsymbol{E}\times\boldsymbol{B}$ drift) suggest long duration for the development. In the morning at high solar activity the EIA develops by ~10:30 LT though the $\boldsymbol{E}\times\boldsymbol{B}$ drift turns upward by 06:30 LT, taking about 240 minutes for the development of EIA. It takes such a long time because in the morning the actual drift is weak and slow varying and ionization production is rapid, so that the slow removal of plasma from around the equator is filled by production. The misinterpretations of EPF and EIA also require long time for the plasma at the equator to drift up in altitude and then diffuse down along the field lines to form EIA.

2.3 EIA under Active Conditions

As mentioned in Section 1, the EIA becomes strong during early (around noon) stages of major geomagnetic storms. The strongest recorded EIA occurred during the extreme storm on 30 October 2003 (e.g., Mannucci et al., 2005), which has been studied in a number of papers (e.g., Lin et al., 2005; Liu et al., 2005; Balan et al., 2011). The strong EIA in electron density N_e measured by CHAMP satellite at ~400 km height during this event (Figure 4a) has a very wide trough, sharp crests at ~±30° latitudes and crest-to-trough ratio ~10; and the density at the crests compared to previous quiet-time values is over 1000%. CHAMP also measured a simultaneous fast equatorward neutral surge (Figure 4b) that crossed over the equator (Balan et al., 2011). Though electric field was not measured during this event, the $\boldsymbol{E}\times\boldsymbol{B}$ drift inferred from the RTI (range time intensity) map of the VHF radar in Brazil (Figure 4c) in nearly same longitude gives the highest recorded upward drift of ~1200 m·s^{-1} (Abdu et al., 2008). The impulsive action of the two drivers together produced the strongest EIA (Figure 4a).

The strong EIA, however, was suggested to be caused by strong eastward PPEF alone. In the fully sunlit equatorial ionosphere the $\boldsymbol{E}\times\boldsymbol{B}$ drift due to eastward PPEF drives plasma upward so fast that it cannot recombine. This plasma spills over into the anomaly, which was suggested to cause the strong EIA (Kelley et al., 2004). This explanation linked to the easy-to-understand pictures of the plasma fountain and EIA was found inadequate because strong eastward PPEF alone cannot strengthen the EIA crests though can produce super plasma fountain and shift the crests to higher latitudes (Balan et al., 2009, 2013).

A storm-time equatorward wind (SEW) with quiet-time $\boldsymbol{E}\times\boldsymbol{B}$ drift (Balan et al., 2010), on the other hand, is found to produce strong EIA as shown in Figure 5a. A SEW produces strong EIA through its mechanical effects that (i) raise and support the ionosphere at high altitudes of reduced chemical loss and (ii) reduce (or stop) downward diffusion of plasma to low altitudes of heavy chemical

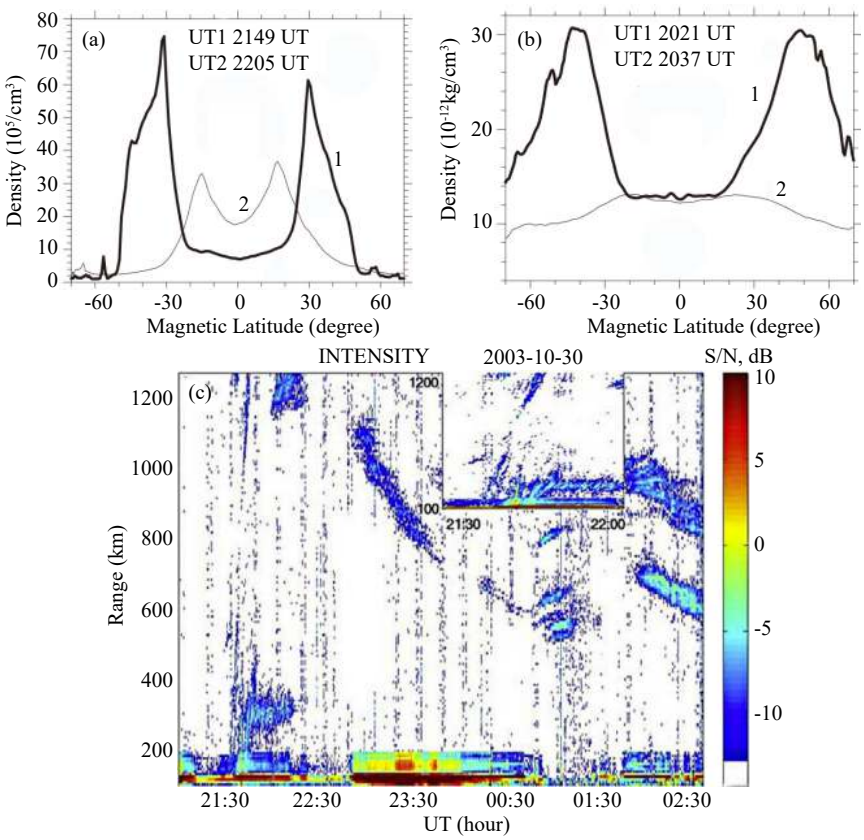

Figure 4. Latitude variations of electron density N_e (a) and neutral density N (b) measured by CHAMP satellite at equatorial crossing time 21:49 UT on 30 October 2003 (curves 1) compared with previous quiet day variations in nearly same crossing time 22:05 UT (curves 2). Positive latitude is north. (c) Shows RTI map of the VHF radar in Brazil on 30 October 2003 (after Abdu et al., 2008).

loss, so that ionization produced during daytime is not lost but are accumulated to strengthen the EIA or produce strong positive ionospheric storms at low and mid latitudes. The optimization of the two mechanical effects together produce strong EIA crests centred at ±16° magnetic latitudes (Balan et al., 2011). In addition to the strong EIA, Figure 5a shows convergence of plasma around the equator which is found to continue during the recovery phase of the storms.

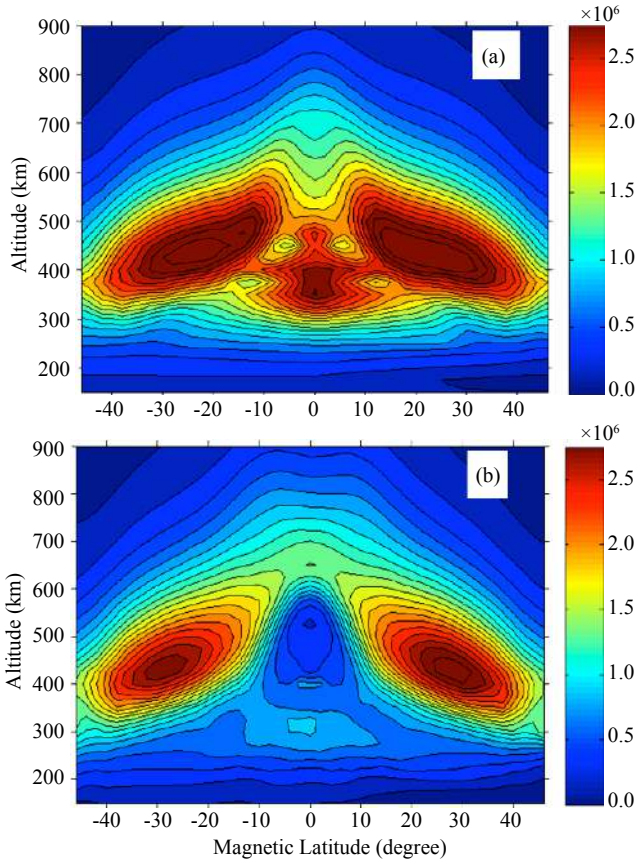

Figure 5. Altitude-latitude variations of electron density N_e at 13:00 LT on 08 November 2004 ($F_{10.7}$ = 123) modelled by SUPIM using (a) equatorward neutral wind and quiet-time ***E***×***B*** drift and (b) equatorward neutral wind and ***E***×***B*** drift due to eastward PPEF. Positive latitude is north (after Balan et al., 2010). Unit of N_e is 10^6 cm^{-3} in both (a) and (b).

When eastward PPEF is also present simultaneously the crests shift poleward (Figure 5b) due to the associated plasma fountain. With the two drivers present together, depending on their strengths, the center of EIA crests can occur between ~±16° and ~±30° magnetic latitudes, which correspond to zero and strong eastward PPEF. When the two drivers (SEW and PPEF) are strong and impulsive the EIA crests will be sharp at around ±30° magnetic latitudes where the poleward moving plasma due to PPEF and equatorward moving plasma due to SEW converge as observed during the extreme storm on 30 October, 2003 (Figure 4a). Detailed explanations of how the impulsive action of the two drivers (strong eastward PPEF and fast equatorward wind) produce the strong EIA have been reported through basic principles, illustrations and detailed model calculations (Balan et al., 2011, 2013).

However, model calculations by SUPIM using eastward PPEF and quiet-time neutral wind during evening hours produced strong EIA, which was interpreted as due to eastward PPEF (Lin et al., 2005). This interpretation is misleading because the quiet-time wind velocity has become equatorward well before the PPEF. Model results by SAMI-2 using eastward PPEF alone showed small strengthening of EIA by about 50% (Huba et al., 2005). Caution is to be taken here not to interpret that strong EIA (over 100% increases in N_{max} and TEC) is also due to eastward PPEF.

The composition change effect of SEW (or O/N_2 decrease) becomes ineffective during early stages of major geomagnetic storms because the ionosphere has already been lifted to high altitudes by the mechanical effect of SEW. However, during later stages (or recovery phase RP) of the storms, the composition change effect of SEW becomes effective and positive ionospheric storms turn to negative storms (Prolss, 1995; Fuller-Rowell et al., 1994). During this time, EIA sometimes gets inhibited with a peak in density at the equator (Sreeja et al., 2009; Tulasi Ram et al., 2008). The equatorial peak during RP has been interpreted as due to westward electric fields (e.g., Huang et al., 2010). But model results (Balan et al., 2013) showed that the equatorial peak occurs mainly due to the convergence of plasma from both hemispheres due to the mechanical effect of SEW with small contributions from westward electric fields and increase in O/N_2 ratio at low latitudes due to the downwelling effect of SEW.

3. Ionospheric Irregularities

3.1 Introduction

The ionosphere has a smooth density distribution during daytime. In other words, during daytime when the E-region conductivity is strong, ionospheric drivers such as neutral winds and electric fields and their fluctuations cannot win in producing irregularities in the ionosphere. But after sunset when the E-region conductivity becomes weak, the drivers can generate plasma irregularities of various scale sizes ranging from centimetres to hundreds of kilometres that manifest as spread-F in ionograms (Booker and Wells, 1938) and plasma bubbles in radar maps (Woodman and Lahoz, 1976) and optical images (Weber et al., 1978). Radio waves propagating through such an irregular ionosphere undergo sporadic enhancement and fading known as scintillations (e.g., Booker, 1956) which affect communication and navigation systems when scintillations are strong.

The irregularities have been studied widely for over 75 years to understand their science and variability and for mitigating their adverse effects on communication and navigation. For extensive reviews see Basu and Basu (1981); Bowman (1990), Aarons (1993), Woodman (2009), and Makela and Otsuka (2012). The irregularities are also called convective ionospheric storms (CIS) which may be more appropriate for their various forms of appearance and underlying physical processes (Kelley et al., 2011). Recently, Yokoyama and Stolle (2017) presented a brief review of the irregularities and reported their effects on geomagnetic field. Here we present a brief review of the studies of the irregularities at low and mid latitudes.

3.1 Low Latitude Irregularities

First observation of irregular plasma density structures in the ionosphere was reported by Booker and Wells (1938) as diffuse ionogram traces at the equatorial station Huancayo in Peru, which came to be known as equatorial spread-F or ESF. Figure 6 shows examples of range spread-F (spread of echoes over a range of virtual heights) and frequency spread-F (spread in frequency for a given virtual height) observed at Huancayo. Booker and Wells (1938) interpreted correctly that the diffuse nature of the echoes is produced by radio wave scattering from electron density fluctuations. Using the incoherent scatter (IS) radar at the equatorial station Jicamarca, Woodman and La Hoz (1976) for the first time reported plasma density depletions extending beyond the ionospheric peak in the region of strong ESF. They interpreted the depletions as the bottom-side irregularities evolving nonlinearly into the topside ionosphere while forming bubble-like structures or equatorial plasma bubbles or EPB. They also suggested that the bubbles will rise by the effect of buoyancy and will continue to do so even in the (topside) regions with gravitationally stable gradients, provided the density inside the bubble is lower than that of the surroundings. This qualitative theory of Woodman and La Hoz (1976) was soon supported by numerical simulations (e.g., Scannapieco and Ossakow, 1976).

Figure 7 shows examples of EPBs observed using the Gadanki radar in India and CHAMP satellite (Patra et al., 2013; Emmert et al., 2010). The radar data show the plasma irregularities origin-

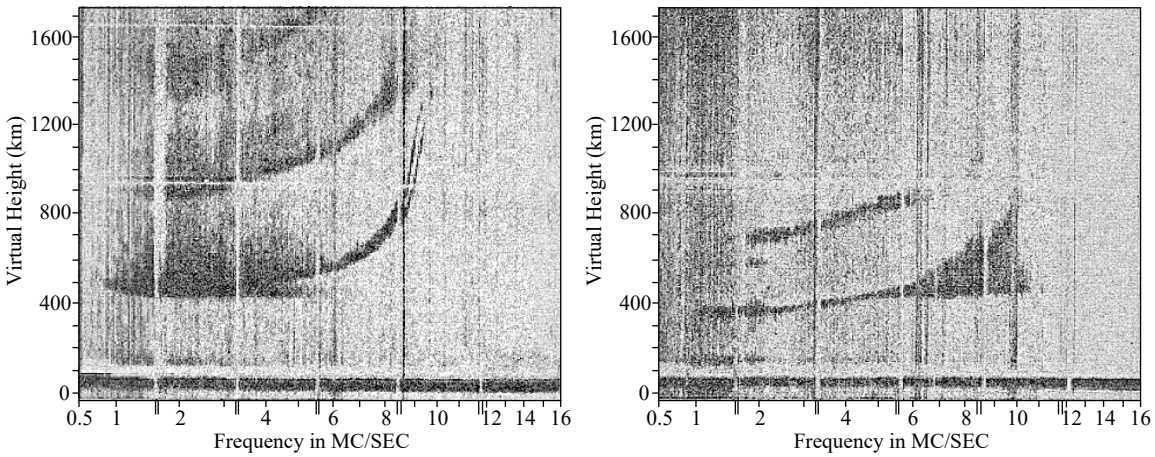

Figure 6. Range spread-F (left) and frequency spread-F (right) at the equatorial station Huancayo (Booker and Wells, 1938).

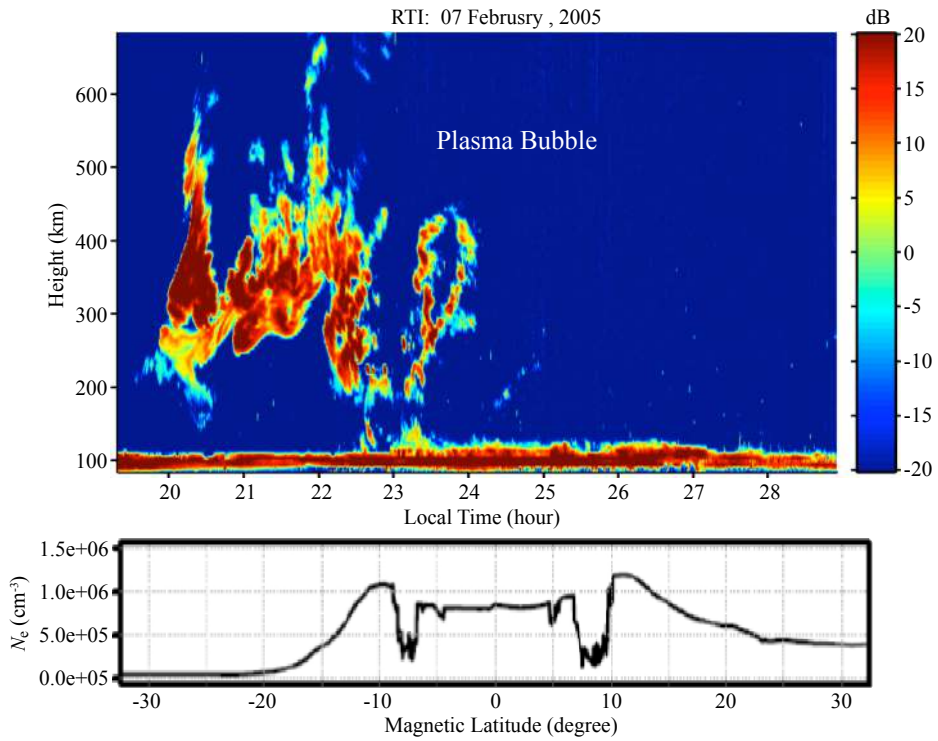

Figure 7. Examples of plasma bubble observed by the Gadanki radar in India on 07 February, 2005 (top, after Patra et al., 2013) and SWARM A satellite on 14 May, 2014; equatorial crossing time is 22:27 UT and longitude is 11° (after Emmert et al., 2010).

ated in the bottom-side raising to high altitudes and evolving into the topside forming bubble-like structures extending sometimes over 700 km height. It also seems to indicate that the irregularities originating at E-region heights pass through the 'forbidden' region of very low plasma density, which the radar seems unable to detect. The CHAMP data show clear signatures of plasma depletions at conjugate locations of approximately ±8° magnetic latitudes. EPBs are also found to drift eastward as shown by an example in Figure 8 obtained using the EAR radar in Indonesia (Ajith et al., 2015). A bubble formed locally in the field-of-view of the radar at 19:51 LT grows in size and drifts eastward with time and disappears from the field-of-view by 21:03 LT. EPBs have been detected in optical images (Weber et al. (1978). As shown in Figure 9, the C/NOFS satellite detected a series of postsunset plasma bubbles around the magnetic equator while transiting through Brazilian longitude. The 630 nm imager in Brazil also detected the plasma bubbles. Otsuka et al. (2002), for the first time, reported identical optical structures at conjugate stations beyond the EIA crests that project to over 2000 km at the equator.

Scintillations of radio waves passing through the irregular ionosphere seem to have been reported first by Booker (1956) and studied in numerous papers (e.g., Basu and Basu, 1981; Bhattacharyya et al., 2001; Li et al., 2007). Figure 10 shows an example of GPS signal undergoing scintillations and loss of track. The schematic illustration shows the signal passing through the regular ionosphere causing range error and irregular ionosphere causing both range error and scintillations. Numerous papers on different aspects of spread-F, plasma bubbles and scintillations under magnetically quiet and active conditions have been reported using ionosondes, radars, optical imagers, rockets and satellites (e.g., Farley et al., 1970; Rastogi et al., 1981; Abdu et al., 1983; Tulasi Ram et al., 2008). Satellite observations, especially, have provided a clear picture of the climatology of the irregularities (e.g., Burke et al., 2004; Stolle et al., 2016; Su et al., 2006).

Plasma irregularities under magnetically active conditions show a mixed picture. In some cases, the irregularities occur and intensify while in some other cases they are inhibited (Aarons, 1991). During the Halloween super storms on 29–30 October, 2003, Sahai et al. (2009) reported that plasma bubbles are generated at the equator and extended to ~33°S magnetic latitudes in South American sector, which maps to ~2500 km over the equator. Tulasi Ram et al. (2008) who studied the irregularities in Indian sector during five storms reported intensification in some cases and inhibition in other cases. Basu et al. (2010) who studied the longitude dependence of VHF scintillations during the main phase (MP) of 30 large storms reported their occurrence in limited longitude sec-

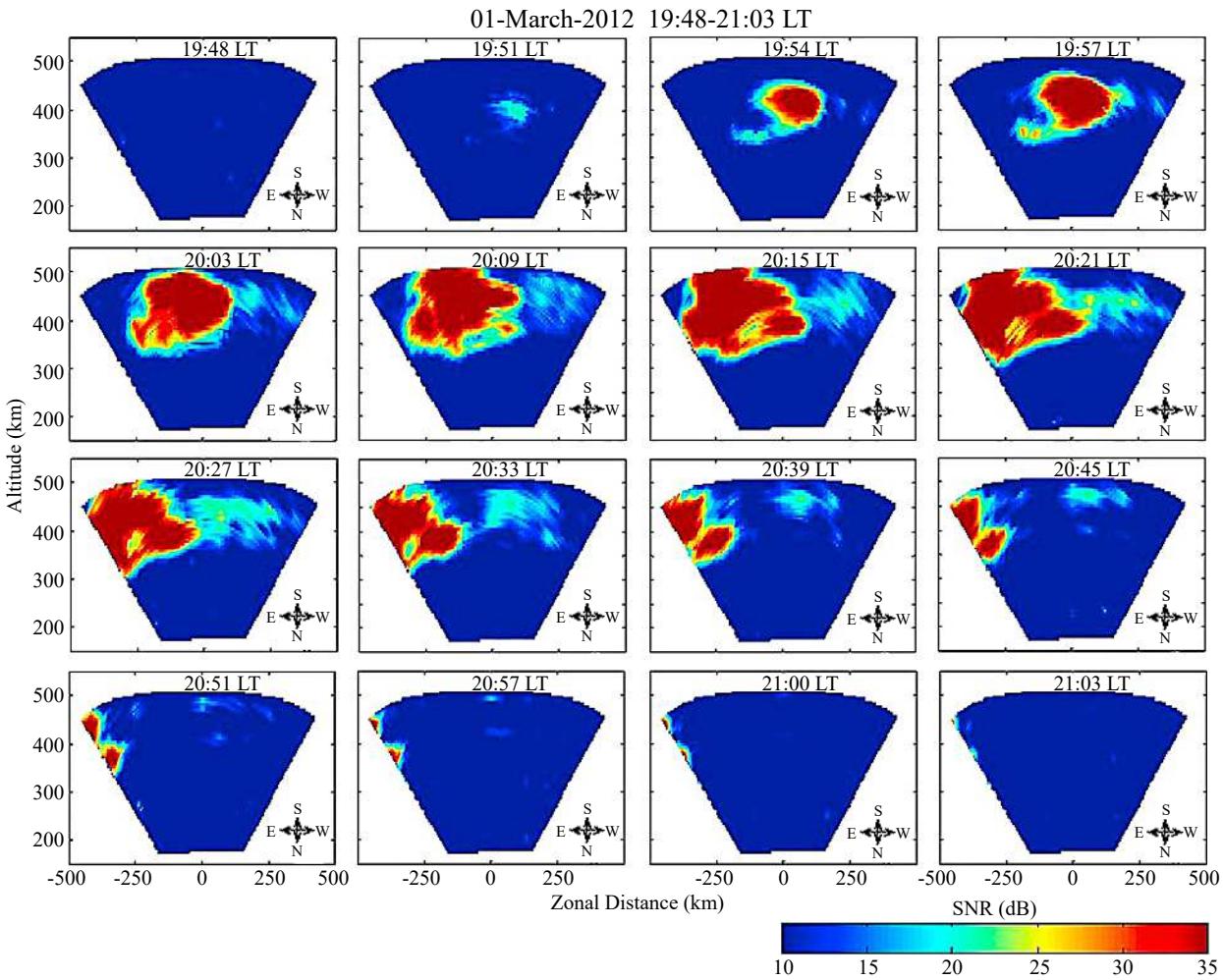

Figure 8. Locally generated bubble drifts eastward in the field of view of the EAR radar in Indonesia (after Ajith et al., 2015).

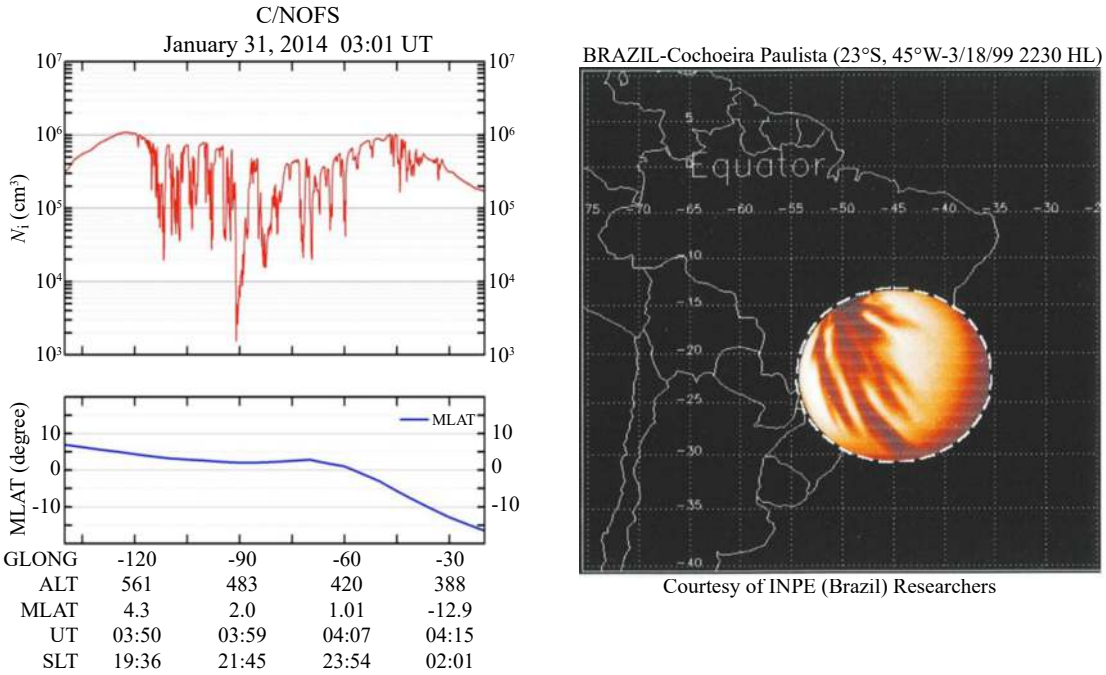

Figure 9. Example of plasma bubble observed by C/NOFS satellite and 630 nm imager (Courtesy of INPE Brazil researchers).

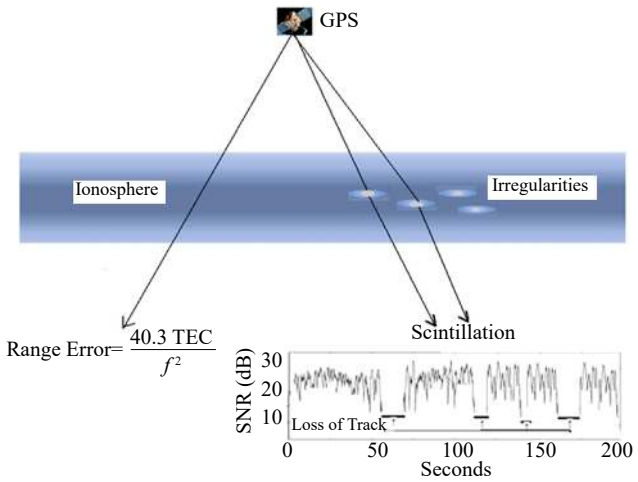

Figure 10. GPS signal undergoing scintillation and loss of track while passing through ionospheirc irregularities.

tors and inhibition in other sectors. Recently, Madhav Haridas et al. (2013) demonstrated the modulation of the growth rate of CRT instability and consequent impact on spread-F occurrence by the enhanced neutral densities during magnetically disturbed periods.

The general features of the irregularities are listed here.

- Plasma irregularities generally occur after ~19:30 LT and continue for about an hour to several hours and sometimes until sunrise.
- Post-sunset irregularities are frequent, intense and last longer centered around the magnetic equator at equinoxes especially at high solar activity.
- In summer and at low solar activity, weak irregularities generally occur after midnight.
- The irregularities usually start appearing in the bottom-side ionosphere when it raises above a threshold height that varies with various geophysical conditions.
- The irregularities quickly rises to high altitudes well beyond the ionospheric peak, sometimes over 2000 km at the equator.
- As the irregularities rise in height they become aligned along the geomagnetic field lines covering up to ±30° magnetic latitudes in extreme cases.
- The irregularities usually drift eastward with velocity of 100 to 200 m·s^{-1}.
- The irregularities causing spread-F can originate at latitudes away from the equator though they do not result in plasma bubbles.
- Geomagnetic activity intensifies the irregularities in some cases and inhibits them in other cases.

3.2 Theory and Modeling

(1) *Theory*

The plasma irregularities at equatorial and low latitudes where geomagnetic field lines are horizontal are thought to originate through the collisional Rayleigh-Taylor (RT) instability mechanism (Dungey, 1956; Balsley et al., 1972), similar to the usual RT instability of a system of a heavy fluid (dense F layer) resting on top of a light fluid (weak E layer). The mechanism that makes it collision-dominated is the post-sunset height rise that raises the ionosphere from its low altitude/high collision/low energy stable state to high altitude/low collision/high energy unstable state.

The paper entitled "Equatorial Spread F: Recent Observations and a New Interpretation" by Balsley et al. (1972) identified the collision-dominated RT (CRT) instability mechanism, which was extended by Haerendel (1972). Unlike the earlier mechanisms (see Farley et al., 1970), the CRT mechanism could account for most of the

observed features of the irregularities such as (1) their close correlation with the height of the bottom-side F layer, (2) their appearance both below and above the F layer peak, and (3) their persistence after the F layer starts drifting downward. The CRT mechanism in essence is —The post-sunset upward motion of the equatorial ionosphere produces severe plasma density depletions in its bottom-side where contours of constant plasma density experience irregular vertical upward and downward motions. In other words, *plasma irregularities develop*. Because the E region has already become weak, these irregularities are not short-circuited. They drift to higher heights with a growth rate (Scannapieco and Ossakow, 1976, equation (3), and V_z added):

$$\gamma = (1/L)\cdot(V_z - g/\nu_{in}) - \beta, \qquad (1)$$

where the term involving V_z is the cross-field instability which dominates in the bottom-side. The term involving g/ν_{in} is the gravity-cum-collisional instability. This term increases exponentially with height due to the decrease of ion-neutral collision frequency ν_{in} and dominates above about 400 km. β is the recombination rate. $L = (1/N_e)\times(dN_e/dz)$ is plasma density scale height. The most important parameter is ν_{in} which determines the dominant role of the height of the F layer. The role of V_z is such that the greater its value, the faster the height rise and hence the quicker the decrease of ν_{in} and faster the growth of the irregularities. The cross-field instability and gravity-cum-collisional instability are in opposite directions and hence the negative sign for the later in equation (1). The theory involving both V_z and g/ν_{in} is referred to as the generalized RT instability.

The main driver that raises the ionosphere in height is the pre-reversal strengthening of the eastward electric field (e.g., Heelis et al., 1974) which causes the pre-reversal enhancement (PRE) of the vertical upward $\boldsymbol{E}\times\boldsymbol{B}$ plasma drift velocity V_z (e.g., Fejer et al., 1979; Namboothiri et al., 1989). As observed by the IS radar at Jicamarca, the irregularities appear when the bottomside F layer rises above a threshold height (Farley et al., 1970). The threshold height was found to depend largely on solar activity. As observed by a HF Doppler radar at 5.5 MHz (Balan et al., 1992), the virtual threshold height (Figure 11) decreases from about 450 km in 1984 to 350 km in 1985 due to the decrease in ν_{in} (Jayachandran et al., 1993).

In addition to the threshold height of the bottom-side, some seeding force was also considered necessary to accelerate the growth rate of the generalized CRT instability (e.g., Kelley et al. 1981). A possible seed mechanism was detected by the HF Doppler radar in its high (1-minute) resolution mode of operation. As shown in Figure 12, the vertical drift velocity V_z always fluctuates and the fluctuations are amplified during PRE (Balachandran Nair et al., 1992). The spectra of the fluctuations obtained on several

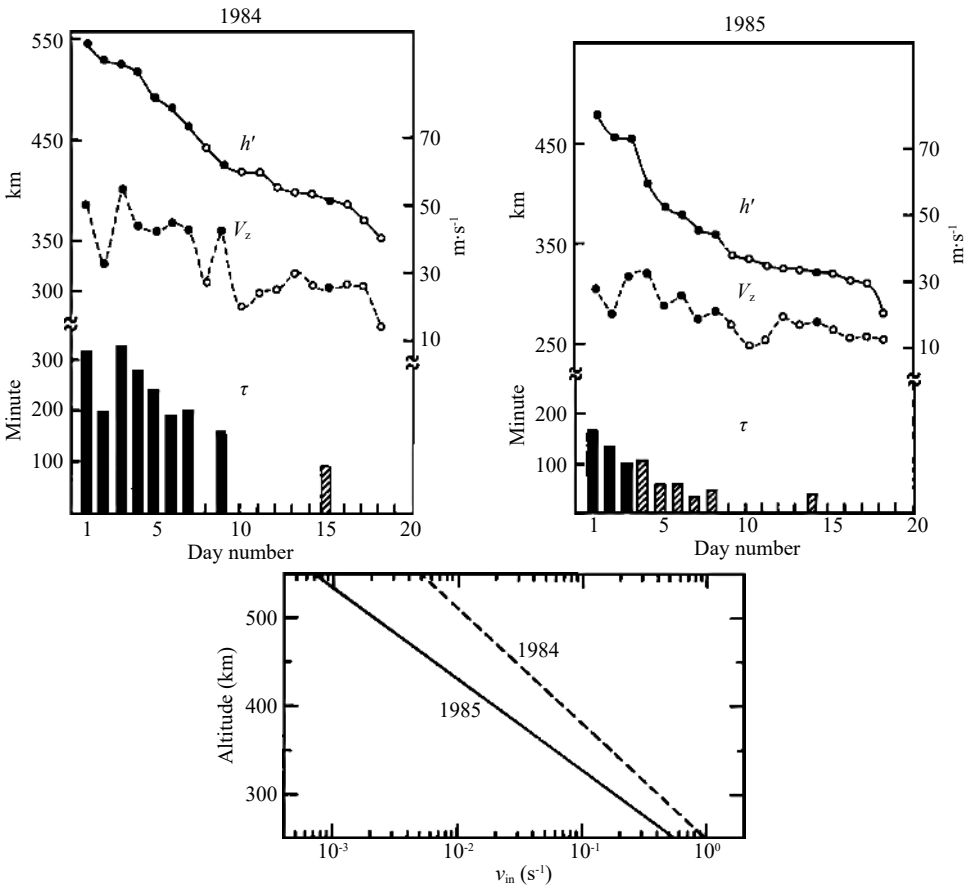

Figure 11. The threshold virtual height *h′* and corresponding vertical drift velocity V_z at the time of onset of ESF arranged in decreasing order of *h′* in March-April 1984 and 1985. The vertical bars indicate duration of ESF. Bottom panel shows the altitude variation of ion-neutral collision frequency in March 1984 and 1985 (from Jayachandran et al., 1993).

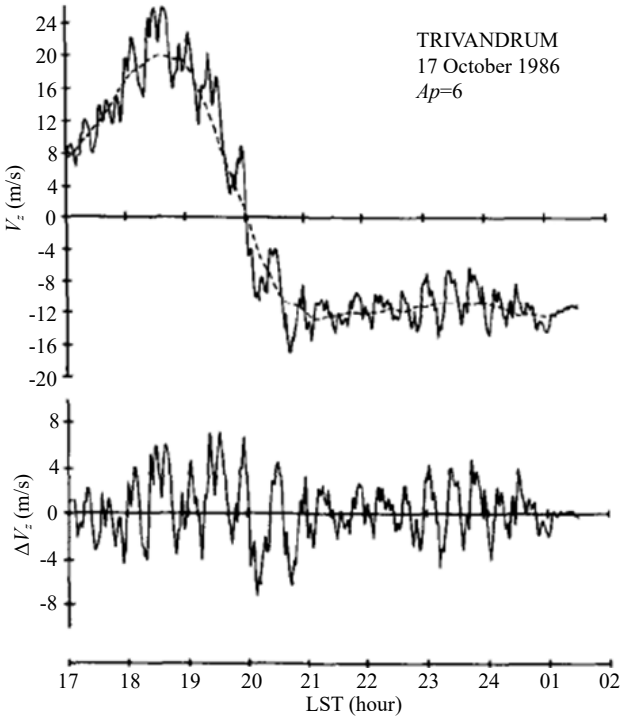

Figure 12. F region (5.5 MHz) vertical plasma drift velocity duirng evening-midnight (top) and amplification of its fluctuations duirng PRE (bottom) (after Balachandran et al., 1992).

days indicate that the dominant fluctuation generally has a period around 30 minutes. Such fluctuations in V_z due to gravity waves including large scale waves (LSW) are thought to act as the seed for the onset of the irregularities (e.g., Prakash, 1999; Tsunoda et al., 2010; Kelley and Dao, 2017).

As the irregularities rise in height they extend along the geomagnetic field lines covering up to ±30° magnetic latitudes in extreme cases. The interhemispheric neutral wind that makes the equatorial ionization anomaly (EIA) asymmetric affects the development and growth of the irregularities. An equatorward wind having negative latitude gradient contributes to destabilizing the ionosphere while a poleward wind does the opposite. The generalised growth rate of the irregularities then has to use the field-line integrated values of the parameters as (Zalesak et al., 1982, equation (45), and R_T added)

$$\gamma_{GD} = (V_z - U_n - g/\nu_{in}) \cdot \Sigma_p^E / [\Sigma_p^{E,S} + \Sigma_p^E + \Sigma_p^{E,N}] \cdot (\Delta N_T / N_T) - R_T. \quad (2)$$

The first three terms (in bracket) are the drift velocities due to electric field, neutral wind and gravity-cum-collision frequency, and last term R_T is the recombination rate. The middle factor includes Pederson conductivities Σ_p^E and Σ_p^F of E and F regions and flux-tube content N_T and its gradient ΔN_T. The effect of this factor is such that the growth rate increases when Σ_p^E sharply decreases around sunset due to dissociative recombination of molecular ions (Sultan, 1996). This also explains the seasonal/longitudinal preference for the irregularity occurrence when the magnetic field declination is aligned with the solar terminator (e.g., Tsunoda, 1985).

Further developments in the theoretical understanding started with the observation by Kudeki and Bhattacharyya (1999) of the existence of a vortex in the plasma drift in bottom-side ionosphere with westward drift in the lower side right before the onset of ESF, which is reproduced in Figure 13. The counter streaming of westward plasma drifts and eastward neutral winds at the bottom of the F-region can provide another important energy source for creating instabilities. Later, Kudeki et al. (2007) obtained comparable growth times using a linear non-local approach including altitude dependent gradients, collision frequencies and sheared plasma drifts. They emphasized that it is the counter streaming rather than the shear that is mainly responsible for the instability. They also postulated that the counter streaming can also provide the seed to the GRT instability for its growth and non-linear development. The importance of the wind is such that it is responsible for (a) the PRE and consequent uplift of the F-layer to more unstable altitudes, (b) the downward reversal of V_z and (c) as a source of instabilities that seed their development.

At low solar activity especially in summer when PRE is absent, the plasma irregularities generally occur at around midnight (e.g., Narayanan et al., 2014; Tulasi Ram et al., 2014) as shown in Figure 14 (Otsuka et al., 2012). They are thought to be caused mainly by the electric field fluctuations due to atmospheric gravity waves including LSW propagating to ionospheric heights (e.g., Tsunoda et al., 2010). The waves originating in convective regions around the equator during daytime grow easily in amplitude as they propagate upward through the rarefied atmosphere and reach high altitudes at later times (late night) at low solar activity compared to high solar activity. The slow varying LSW can act as both driver and seed during post-midnight hours when the fast varying PRE is absent. The plasma density after postsunset hours is also low especially at solar minimum, which could also contribute to the growth of the irregularities through the scale height factor.

During geomagnetic storms additional drivers arise due to solar wind-magnetosphere-ionosphere coupling, which largely modify the back-ground ionosphere-thermosphere system (e.g, Balan et al., 2010, 2013). The additional drivers include prompt penetration electric field (PPEF) from high latitudes (Rastogi, 1977), disturbance dynamo electric field (DDEF) due to storm-time neutral wind, and storm-time equatorward neutral winds and waves. The PPEF is eastward/westward for southward/northward IMF B_z until around 19:00 LT and the directions reverse afterwards (Kikuchi et al., 1978). The DDEF on the other hand is westward on dayside and eastward on night side (Blanc and Richmond, 1980). The storm-time winds and waves are equatorward and westward (Balan et al., 2011). Depending mainly on the time of onset of geomagnetic storms, the additional drivers can become in phase or out of phase with quiet-time drivers, which results in a highly unpredictable situation for the occurrence of the irregularities.

The day-to-day variability of the irregularities is such that even at around the peak of the equinox season when the irregularities occur on most nights they do not occur on some nights even though PRE and altitude exceed their threshold values (e.g., Jayachandran et al., 1987; Balan et al., 2018). Attempts have been made to forecast the occurrence of the irregularities several hours

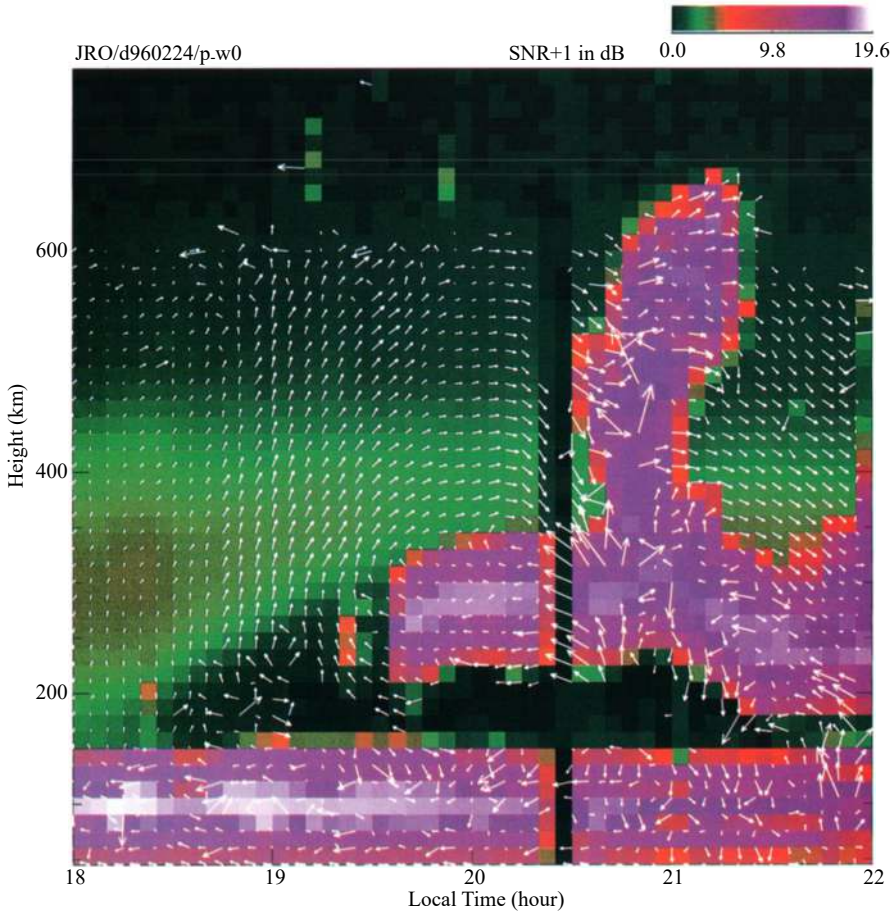

Figure 13. RTI plot showing spread-F echoes (purple color), electron density (Greenish tones) and vector drifts. Note the very clear vector drifts in the F-region. The main feature of this image is the existence of a vortex at the bottom of F-region, with westward drifts in the lower side, right before the initiation of bottom-side spread-F echoes (after Kudeki and Bhattacharyya, 1999).

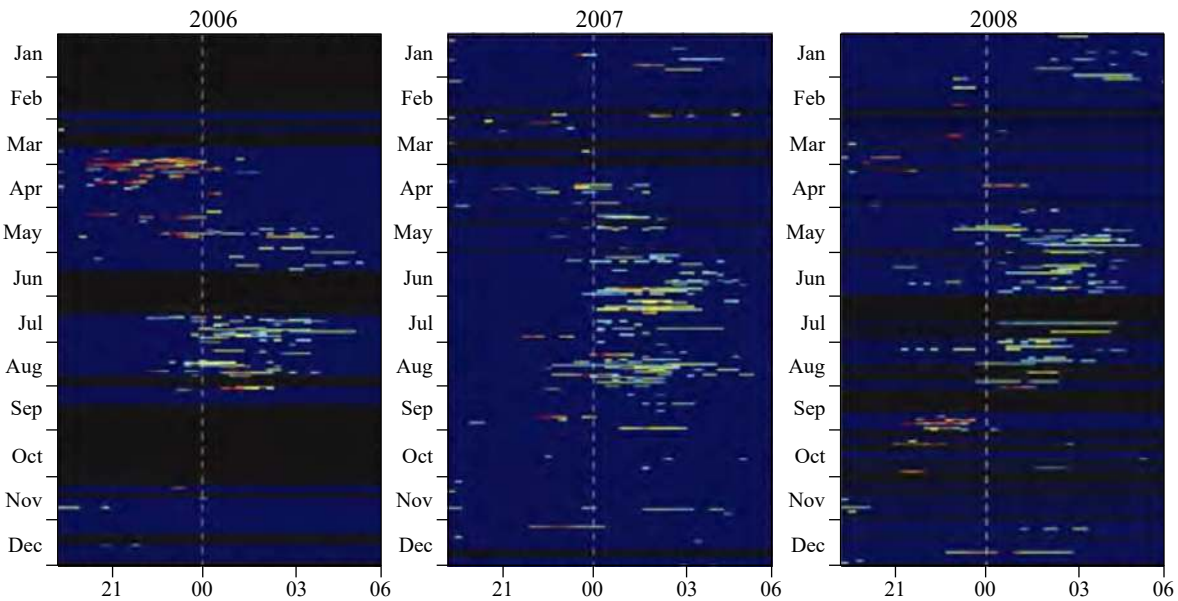

Figure 14. Plasma irregularities in month-local time frame observed by VHF radar (after Otsuka et al., 2012).

in advance. For example, Thampi et al. (2006) used the strength and asymmetry of afternoon EIA with some success. Recently, Anderson and Redmon (2017) used $h'F_{1930}$ (minimum virtual height of bottom-side at 19:30 LT) with 80% success. Aswathy and Manju

(2018) used an empirical approach to hindcast equatorial spread F irregularities in the electrodynamical regime with ~96% success.

(2) *Modelling*

As mentioned above, to explain the first plasma bubble observed above the ionospheric peak using the Jicamarca radar, Woodman and La Hoz (1976) proposed that the bottom-side irregularities evolve nonlinearly into the topside ionosphere while forming EPBs. The concept of EPB penetrating to the topside was supported by 2-D numerical simulations on magnetic equatorial planes (Scannapieco and Ossakow, 1976; Zalesak et al., 1982) and has been widely accepted. In earlier models using steady V_z, the seed for the onset of the irregularities has been artificially introduced as a small initial perturbation (5%) of the electron density contours.

The artificial seeding can be avoided when actual V_z having natural fluctuations (due to gravity waves) of sufficient amplitude as observed (e.g., Figure 12) is used. Figure 15 (left panel) shows an example of plasma bubble simulated by Sekar et al. (1995) using 0.5% initial perturbation and fluctuating V_z; it corresponds to 1200 seconds after the start of simulation. The right hand panel of Figure 15 is from Huang and Kelley (1996) who simulated the plasma bubble using fluctuating V_z and no initial perturbation; it corresponds to 1920 seconds after the start of simulation. In both cases, the irregularities originate in the bottom-side and evolve non-linearly into the topside, illustrating the importance of gravity wave seeding of plasma irregularities.

Recently, various 3-D numerical models have been available to study the plasma irregularities (e.g., Huba et al., 2008; Aveiro and Hysell, 2011). Figure 16 is an example of EPB development modeled using the 3-D HIRB (high resolution bubble) model (Yokoyama et al., 2014). A sinusoidal perturbation as an initial seeding is applied by raising the density profile perpendicular to the magnetic field. As the bubble rises up in height at the equator, they extend along the horizontal plane, and the bubble bifurcates into small scale structures in the topside. As commented by Yokoyama and Stolle (2017), regional models such as HIRB are not capable of simulating a realistic background condition in which, for example, a nighttime (daytime) condition should be applied at the eastern (western) boundary around the dusk terminator. To overcome the shortcoming of the regional models, significant progress could be achieved by integrating them into global atmosphere-ionosphere coupled models, in which all necessary parameters are available without specific boundary conditions. Recent numerical simulations initialized by observational data before the onset of EPBs have successfully reproduced the day-to-day variability of EPB occurrence (Hysell et al., 2014).

Earlier model calculations of the growth rate have predicted a low latitude minimum for the occurrence of the irregularities. For example, Maruyama (1990) who calculated the growth rate of both the gravitational and cross-field instability modes using flux tube integrated values (without neutral wind) showed that the net instability growth rate at March equinox under medium solar activity ($F_{10.7}$ = 120) is negative in a narrow latitude region near 18° magnetic latitudes. At lower and higher latitudes, the ionosphere becomes unstable. The possibility of the minimum has also been indicated by the observations of mid-latitude MSTIDs (Shiokawa et al., 2002), which show a low-latitude limit for their propagation at ~18°N magnetic latitudes at high solar activity (1999); and the limit extends to further lower latitudes at low solar activity (e.g., Narayanan et al., 2014).

3.3 Mid Latitudes Irregularities

Plasma irregularities have been observed at mid latitudes as shown in Figure 17. Bowman made extensive studies of mid latitude irregularities which were summarised in his review article (Bowman, 1990). Whalen (2002) studied the spread-F occurrence at a chain of stations up to 20° magnetic latitudes in American sector. Fukao et al. (1991) studied the F-region plasma irregularities observed by the MU (middle and upper atmosphere) radar in Japan.

The plasma irregularities at mid latitudes were first thought to be associated with atmospheric gravity waves (e.g., Bowman, 1990;

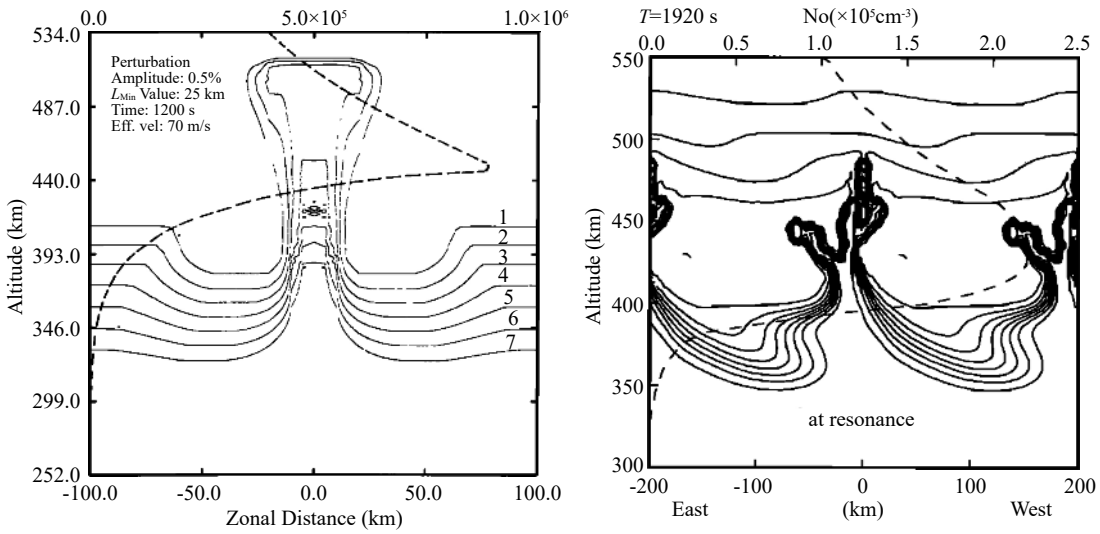

Figure 15. Plasma bubbles simulated by Sekar et al. (1995) using 0.5% initial perturbation and fluctuating drift velocity due to gravity waves (left) and Huang and Kelley (1996) using fluctuating drift velocity and no initial perturbation.

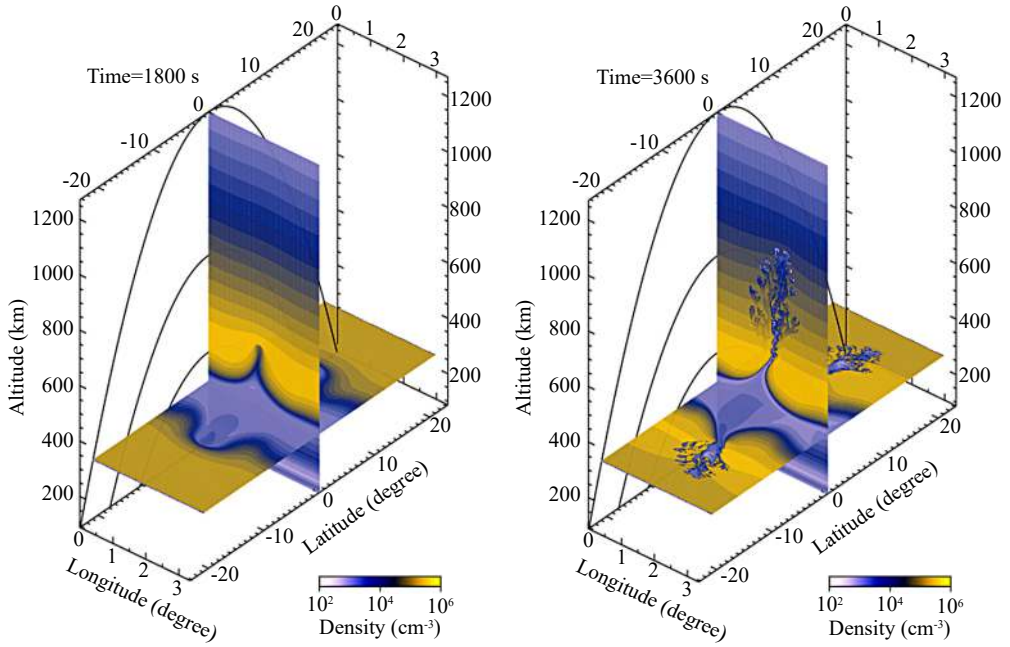

Figure 16. Model development of Plasma bubbles in 3-D. Figure shows the plasma density distribution in 3-D domain at 1800 and 3600 secs after the start of simulation. Longitude-altitude planes at the equator and horizontal planes at an altitude of 300 km are shown (after Yokoyama et al., 2014).

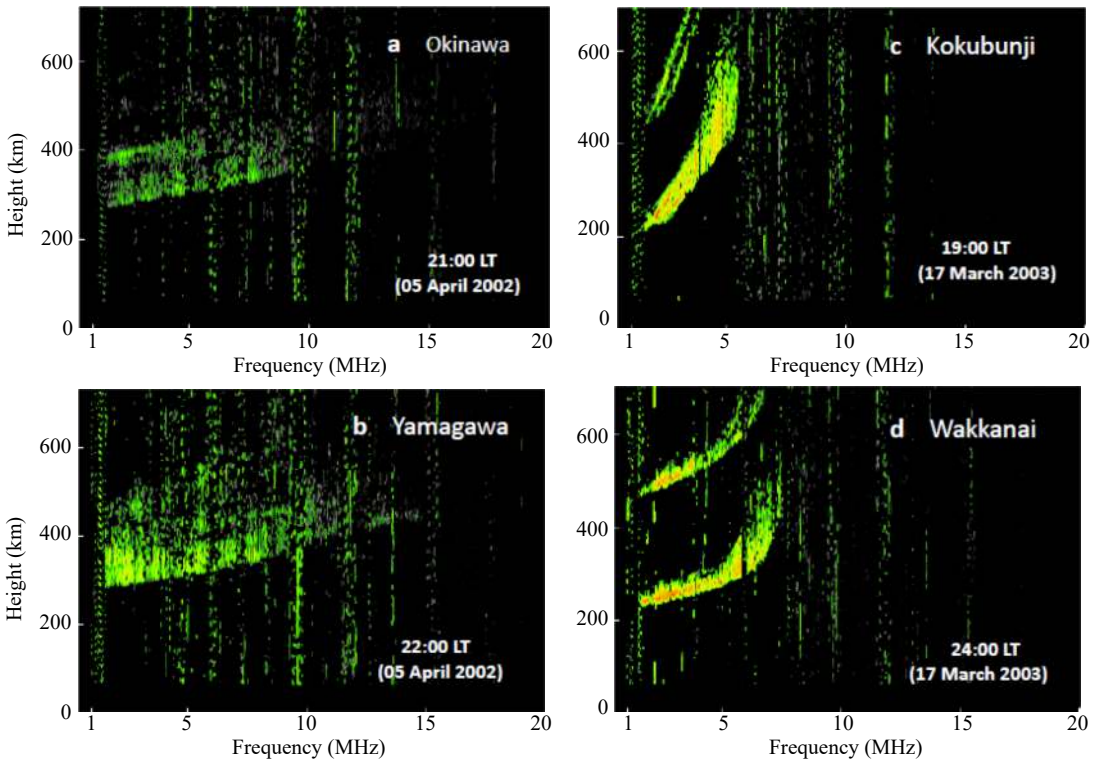

Figure 17. Spread-F at low and mid latitudes. The sample ionograms illustrate range type spread-F at low latitude stations (a) Okinawa (26.3°N, 127.6°E; 15.3°N magnetic latitudes.) and (b) Yamagawa (31.2°N, 130.6°E; 21.2°N) on 05 April 2002 (Ap = 4) and more of frequency type spread-F at mid latitude stations (c) Kokubunji (35.7°N, 139.5°E; 26.5°N) and (d) Wakanai (45.4°N, 141.7°E; 36.5°N) on 17 March 2003 (Ap = 42) in Japan (Balan et al., 2018).

Kelley and Fukao, 1991) and later with medium-scale travelling ionospheric (atmospheric) disturbances (MSTIDs) (e.g., Makela and Otsuka, 2012). The mechanism that relates the mid latitude plasma irregularities to its source (e.g., MSTID) is the so-called Per-

kins instability (Perkins, 1973) which takes the form of rising and falling sheets of ionization when a north-south electric field is present in addition to the east-west field. Hamza (1999) updated the Perkins equations by adding neutral wind. Recent understanding is that the electro-dynamical coupling between the E- and F-regions plays an important role in enhancing the growth rate of Perkins instability (e.g., Tsunoda and Cosgrove, 2001). The instability has a linear growth rate (Tsunoda, 2006; Yokoyama and Stolle, 2017).

$$\gamma = (|\boldsymbol{E}|\cos I)\,[\sin(\theta-\alpha)\sin\alpha]\,/\,\boldsymbol{B}H, \qquad (3)$$

where $\boldsymbol{E} = \boldsymbol{E}_0 + \boldsymbol{U}^{\mathrm{F}}\times\boldsymbol{B}$ is total effective electric field with $\boldsymbol{E}_0$ being the background field; $\boldsymbol{U}^{\mathrm{F}}$ is F-region neutral wind, $\boldsymbol{B}$ is geomagnetic field of magnitude B, I is magnetic inclination angle, H is atmospheric scale height including ion-neutral collision frequency, θ is the angle between $\boldsymbol{E}$ and east direction, and α is the angle between the direction normal to the frontal structure and east direction. A maximum in the growth rate γ is expected to occur at the location where $\alpha = \theta/2$. Such a maximum is also expected from the latitude variation of MSTIDs which have maximum occurrence at mid latitudes and no occurrence at latitudes below ~18°N magnetic latitudes at high solar activity (Shiokawa et al., 2002).

As discussed in Sections 2 and 3, theoretical models have predicted a low-latitude minimum (e.g., Maruyama, 1990) and a mid-latitude maximum (e.g., Tsunoda, 2006) for the occurrence of plasma irregularities. The location of the spread-F minimum has recently been identified by analysing the ionosonde data at four low to mid latitude locations (17.0°N, 21.2°N, 26.5°N and 36.5°N magnetic latitudes) in Japan longitude sector (~135°E) in March–April 2002, 2003, and 2006 (high, medium and low solar activity). As shown in Figure 18, the spread-F occurrence under medium solar activity (2003) has a minimum (30%) near Yamagawa (21.2°N) and maximum (60%) near or beyond Wakkanai (36.5°N); and the occurrence on the equatorward side (Okinawa, (40%) is greater than that at the minimum. Considering all three levels of solar activity, the spread F minimum occurs on the poleward side of the EIA crest and shifts equatorward from ~25°N magnetic latitudes at high solar activity to 17°N at low solar activity (Balan et al., 2018). The corresponding spread-F maximum occurring on the poleward side of the minimum is also found to shift equatorward from ~35°N (or beyond) at medium solar activity to 20°N–25°N at low solar activity, and no spread-F was observed on the poleward side of the minimum at high solar activity. The spread-F at latitudes equatorward of the minimum seems to be of CRT mechanism while that on the poleward side is mainly of Perkins mechanism.

4. Summary

A brief review has been presented on the recent developments in the understanding of two major phenomena in Earth's ionosphere at low to mid latitudes —The equatorial ionization anomaly (EIA) and involved equatorial plasma fountain (EPF) and ionospheric irregularities. The main points are summarised.

4.1 Equatorial Ionization Anomaly

The EIA develops in the morning, continues to exist well beyond sunset and covers up to half the global area in 24 hours. Though theoretical models have reproduced the EIA and its variations long ago, the easy-to-understand misinterpretations of the EPF and EIA have caused misunderstandings both under quiet and active conditions. The misunderstandings are clarified.

It is clarified that the EPF is not upward $\boldsymbol{E}\times\boldsymbol{B}$ plasma drift at the equator followed by downward plasma diffusion along the field lines, but it is field perpendicular $\boldsymbol{E}\times\boldsymbol{B}$ plasma drift and field-aligned plasma diffusion acting together all along the field lines at all altitudes, and plasma flowing in the direction of the resultant. The EIA is formed not from the accumulation of plasma at the crests but mainly from the removal of plasma from around the equator by the upward $\boldsymbol{E}\times\boldsymbol{B}$ drift creating the trough and consequently the crests with small accumulation at the crests when the crests are within ~±20° magnetic latitudes and no accumulation when they are beyond ~±25°. The time required for the development of EIA is less than the time expected from the easy-to-understand misinterpretations.

During early stages of the daytime (around noon) main phase of major geomagnetic storms the plasma fountain becomes a super fountain and EIA becomes strong not due to eastward prompt penetration electric field (PPEF) alone but due to the combined impulsive action of both eastward PPEF and storm-time equatorward winds (SEW). SEW (with normal electric field) alone can produce strong EIA while PPEF alone is unlikely.

4.2 Ionospheric Irregularities

Ionospheric irregularities generally appear as spread-F after 19:30 LT and continue for about one hour to several hours and sometimes until sunrise. Generally, intense irregularities occur at high and medium solar activity in the equatorial ionosphere where geomagnetic field lines are horizontal and weak irregularities occur at higher latitudes where field lines are inclined. The intense irregularities develop in the post-sunset bottom-side ionosphere when it raises to high altitudes, and evolve nonlinearly into the topside as plasma bubbles. Radio waves passing through the irregularities undergo scintillations having adverse effects on communication and navigation.

Pre-reversal enhancement (PRE) of the vertical upward $\boldsymbol{E}\times\boldsymbol{B}$ drift and its fluctuations amplified during PRE provide the driving force and seed for the collisional RT instability mechanism for the intense irregularities, with neutral wind and gravity waves being the primary sources. The neutral wind in the bottom-side itself seems to do the job of seeding. At low solar activity especially in summer when the fast varying PRE is absent, the slow varying gravity waves including large scale waves (LSW) seem to act as both driver and seed for weak irregularities. Geomagnetic activity intensifies the irregularities in some cases and inhibits them in other cases. At mid latitudes, the irregularities are weak and associated with medium scale traveling ionospheric disturbances (MSTIDs) through Perkins instability mechanism.

Theoretical models have predicted a low latitude minimum and a mid-latitude maximum for the occurrence of the irregularities. The locations of the minimum and maximum are identified using the ionosondes in Japan longitude. The minimum occurs on the poleward side of the EIA crest and shifts equatorward from ~25° mag-

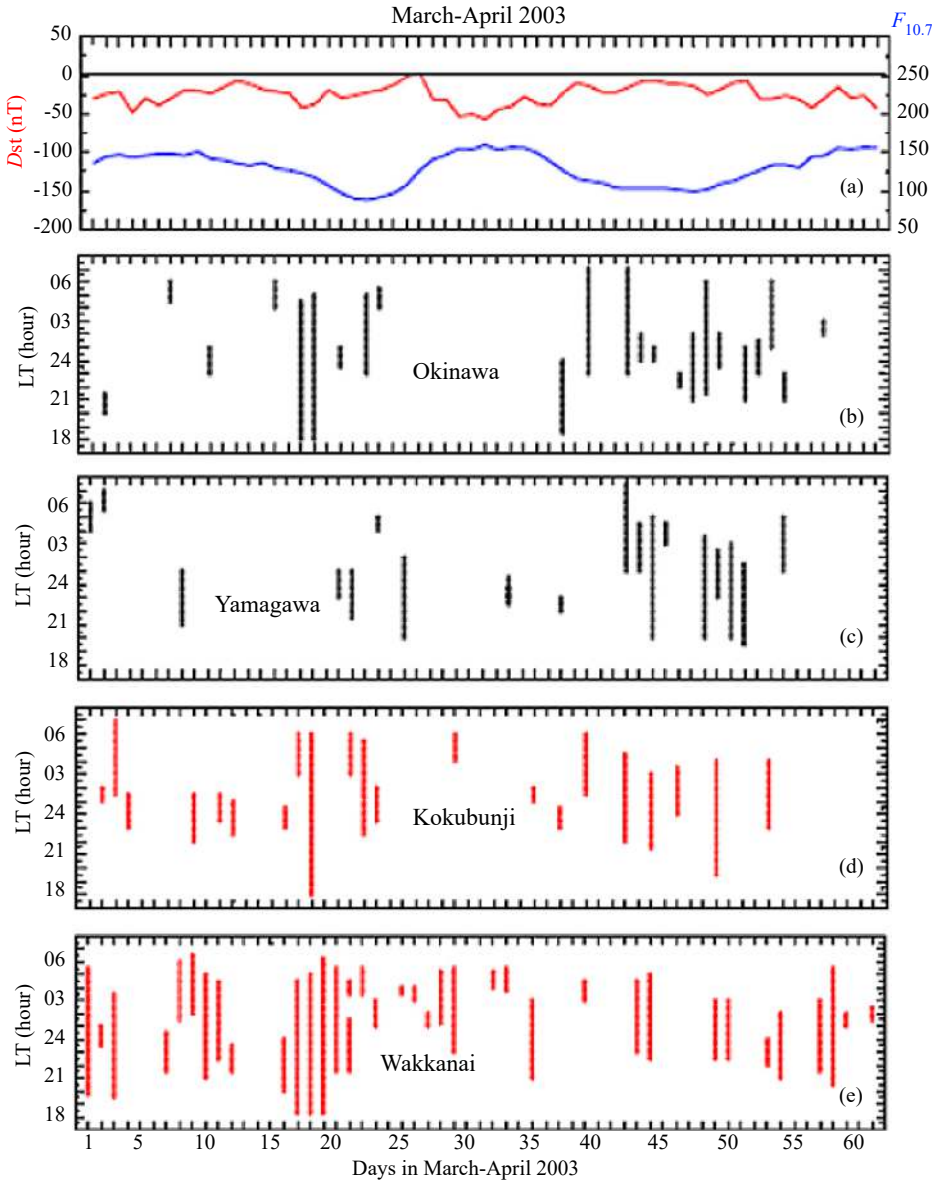

Figure 18. Occurrence of spread F at four locations (17.0°N, 21.2°N, 26.5°N and 36.5°N magnetic latitudes from top) in Japan in March–April 2003 showing a clear low latitude minimum near 20°N (Yamagawa) and a mid-latitude maximum near or beyond 35°N (Wakkanai) (after Balan et al., 2018).

netic latitudes at high solar activity to below 17° at low solar activity. The corresponding mid-latitude maximum also shifts equatorward with decreasing solar activity.

The studied of the irregularities need to be continued for an in depth understanding of their day-to-day variations to reach a level of forecasting capability. One possible approach seems—continuously monitor the state of the ionosphere and thermosphere from mesopause level and incorporate the current states into models to simulate the irregularities. With such an approach for one spread-F season, by observing the states alone until 15:00 LT, it could most probably be possible to forecast weather the (intense) irregularities are going to occur or not.

Acknowledgements

Numerous papers on the EIA and ionospheric irregularities under quiet and active conditions have been published by various research groups around the world though a limited number of them could be referred in this brief review. N. Balan thanks IGGCAS at Beijing (China) for a visiting professor position. The ionosonde data used are obtained using the ionosondes in Japan, which are available at http://wdc.nict.go.jp/ionog/js_viewer/js_01.html. This work was supported by National Natural Science Foundation of China (41621063, 41774161) and the Open Research Project of Large Research Infrastructures of CAS—"Study on the interaction between low/mid-latitude atmosphere and ionosphere based on the Chinese Meridian Project".

References

Aarons, J. (1991). The role of the ring current in the generation or inhibition of equatorial F layer irregularities during magnetic storms. *Radio Sci.*, *26*(4), 1131–1149. https://doi.org/10.1029/91RS00473

Aarons, J. (1993). The longitudinal morphology of equatorial F-layer irregularities relevant to their occurrence. *Space Sci. Rev.*, *63*(3-4), 209–243. https://doi.org/10.1007/BF00750769

Abdu, M. A., de Medeiros, R. T., Bittencourt, J. A., and Batista, I. S. (1983). Vertical ionization drift velocities and range type spread F in the evening equatorial ionosphere. *J. Geophys. Res.*, *88*(A1), 399–402. https://doi.org/10.1029/JA088iA01p00399

Abdu, M. A., de Paula, E. R., Batista, I. S., Reinisch, B. W., Matsuoka, M. T., Camargo, P. O., Veliz, O., Denardini, C. M., Sobral, J. H. A., … de Siqueira P. M. (2008). Abnormal evening vertical plasma drift and effects on ESF and EIA over Brazil-South Atlantic sector during the 30 October 2003 superstorm. *J. Geophys. Res.*, *113*(A7), A07313. https://doi.org/10.1029/2007JA012844

Ajith, K. K., Ram, S. T., Yamamoto, M., Yokoyama, T., Gowtam, V. S., Otsuka, Y., Tsugawa, T., and Niranjan, K. (2015). Explicit characteristics of evolutionary-type plasma bubbles observed from Equatorial Atmosphere Radar during the low to moderate solar activity years 2010-2012. *J. Geophys. Res. Space Phys.*, *120*(2), 1371–1382. https://doi.org/10.1002/2014JA020878

Anderson, D. N. (1973). A theoretical study of the ionospheric F region equatorial anomaly-I. *Theory. Planet. Space Sci.*, *21*(3), 409–419. https://doi.org/10.1016/0032-0633(73)90040-8

Anderson, D. N., and Redmon, R. J. (2017). Forecasting scintillation activity and equatorial spread F. *Space Weather*, *15*(3), 495–502. https://doi.org/10.1002/2016SW001554

Appleton, E., and Barnett, M. (1925). Local reflection of wireless waves from the upper atmosphere. *Nature*, *115*(2888), 333–334. https://doi.org/10.1038/115333a0

Appleton, E. V. (1946). Two anomalies in the ionosphere. *Nature*, *157*(3995), 691. https://doi.org/10.1038/157691a0

Aswathy, R. P., and Manju, G. (2018). Hindcasting of equatorial spread F using seasonal empirical models. *J. Geophys. Res.*, *123*(2). https://doi.org/10.1002/2017JA025036

Aveiro, H. C., Hysell, D. L., Park, J., and Lühr, H. (2011). Equatorial spread F-related currents: three-dimensional simulations and observations. *Geophys. Res. Lett.*, *38*(21), L21103. https://doi.org/10.1029/2011GL049586

Bailey, G. J., and Balan, N. (1996). A low latitude Ionosphere-plasmasphere model. In R. W. Schunk (Ed.), STEP Hand Book of Ionospheric Models (pp. 173). Logan: Utah State University.

Balachandran Nair, R., Balan, N., Bailey, G. J., and Rao, P. B. (1992). Spectra of the ac electric fields in the post-sunset F-region at the magnetic equator. *Planet. Space Sci.*, *40*(5), 655–662. https://doi.org/10.1016/0032-0633(92)90006-A

Balan, N., Jayachandran, B., Balachandran Nair, R., Namboothiri, S. P., Bailey, G. J. and Rao, P. B. (1992). HF Doppler observations of vector plasma drifts in the evening F-region at the magnetic equator. *J. Atoms. Terr. Phys.*, *54*(11-12), 1545–1554. https://doi.org/10.1016/0021-9169(92)90162-E

Balan, N., and Bailey, G. J. (1995). Equatorial plasma fountain and its effects: possibility of an additional layer. *J. Geophys. Res.*, *100*(A11), 21421–21432. https://doi.org/10.1029/95JA01555

Balan, N, Bailey, G. J., Abdu, M. A., Oyama, K. I., Richards, P. G., MacDougall, J., and Batista, I. S. (1997). Equatorial plasma fountain and its effects over three locations: Evidence for an additional layer, the F3 layer. *J. Geophys. Res.*, *102*(A2), 2047–2056. https://doi.org/10.1029/95JA02639

Balan, N., Batista, I. S., Abdu, M. A., MacDougall, J., and Bailey, G. J. (1998). Physical mechanism and statistics of occurrence of an additional layer in the equatorial ionosphere. *J. Geophys. Res.*, *103*(A12), 29169–29181. https://doi.org/10.1029/98JA02823

Balan, N., Shiokawa, K., Otsuka, Y., Watanabe, S., and Bailey, G. J. (2009). Super plasma fountain and equatorial ionization anomaly during penetration electric field. *J. Geophys. Res.*, *114*(A3), A03310. https://doi.org/10.1029/2008JA013768

Balan, N., Shiokawa, K., Otsuka, Y., Kikuchi, T., Vijaya Lekshmi, D., Kawamura, S., Yamamoto M., and Bailey, G. J. (2010). A physical mechanism of positive ionospheric storms at low latitudes and midlatitudes. *J. Geophy. Res.*, *115*(A2), A02304. https://doi.org/10.1029/2009JA014515

Balan, N., Yamamoto, M., Liu, J. Y., Otsuak, Y., Liu, H., and Lühr, H. (2011). New aspects of thermospheric and ionospheric storms revealed by CHAMP. *J. Geophys. Res.*, *116*(A7), A07305. https://doi.org/10.1029/2010JA016399

Balan, N., Otsuka, Y., Nishioka, M., Liu, J. Y., and Bailey, G. J. (2013). Physical mechanisms of the ionospheric storms at equatorial and higher latitudes during the recovery phase of geomagnetic storms. *J. Geophys. Res.*, *118*(5), 2660–2669. https://doi.org/10.1002/jgra.50275

Balan, N., Maruyama, T., Patra, A. K., and Narayanan, V. L. (2018). A minimum in the latitude variation of spread-F at March equinox. *Prog. Earth Planet. Sci.*, *5*, 27. https://doi.org/10.1186/s40645-018-0180-y

Balsley, B. B., Haerendel, G., and Greenwald, R. A. (1972). Equatorial spread F: Recent observations and a new interpretation. *J. Geophys. Res.*, *77*(28), 5625–5628. https://doi.org/10.1029/JA077i028p05625

Basu, S., and Basu, S. (1981). Equatorial scintillation-a review. *J. Atmos. Terr. Phys.*, *43*(5-6), 473–489. https://doi.org/10.1016/0021-9169(81)90110-0

Basu, S., Basu, S., MacKenzie, E., Bridgwood, C., Valladares, C. E., Groves, K. M., and Carrano, C. (2010). Specification of the occurrence of equatorial ionospheric scintillations during the main phase of large magnetic storms within solar cycle 23. *Radio Sci.*, *45*(5), RS5009. https://doi.org/10.1029/2009RS004343

Beynon, W. J. G. (1975). Marconi, radio waves, and the ionosphere. *Radio Sci.*, *10*(7), 657–664. https://doi.org/10.1029/RS010i007p00657

Bhattacharyya, A., Basu, S., Groves, K. M., Valladares, C. E., and Sheehan, R. (2001). Dynamics of equatorial F region irregularities from spaced receiver scintillation observations. *Geophys. Res. Lett.*, *28*(1), 119–122. https://doi.org/10.1029/2000GL012288

Blanc, M., and Richmond, A. D. (1980). The ionospheric disturbance dynamo. *J. Geophys. Res.*, *85*(A4), 1669–1686. https://doi.org/10.1029/JA085iA04p01669

Booker, H. G., and Wells, H. W. (1938). Scattering of radio waves by the F-region of the ionosphere. *Terr. Magn. Atmos. Elec.*, *43*(3), 249–256. https://doi.org/10.1029/TE043i003p00249

Booker, H. G. (1956). Turbulence in the ionosphere with applications to meteor-trails, radio-star scintillation, auroral radar echoes, and other phenomena. *J. Gephys. Res.*, *61*(4), 673–705. https://doi.org/10.1029/JZ061i004p00673

Bowman, G. G. (1990). A review of some recent work on mid-latitude spread-F occurrence as detected by ionosondes. *J. Geomagn. Geoelectr.*, *42*(2), 109–138. https://doi.org/10.5636/jgg.42.109

Breit, G., and Tuve, M. A. (1925). A radio method of estimating the height of the conducting layer. *Nature*, *116*(2914), 357. https://doi.org/10.1038/116357a0

Burke, W. J., Gentile, L. C., Huang, C. Y., Valladares, C. E., and Su, S. Y. (2004). Longitudinal variability of equatorial plasma bubbles observed by DMSP and ROCSAT-1. *J. Geophys. Res.*, *109*(A12), A12301. https://doi.org/10.1029/2004JA010583

Chapman, S. (1931). The absorption and dissociative or ionizing effect of monochromatic radiation in an atmosphere on a rotating earth. *Proc. Phys. Soc.*, *43*(1), 26–45. https://doi.org/10.1088/0959-5309/43/1/305

Chen, Y. D., Liu, L. B., Le, H. J., Wan, W. X., and Zhang, H. (2016). Equatorial ionization anomaly in the low-latitude topside ionosphere: Local time evolution and longitudinal difference. *J. Geophys. Res.*, *121*(7), 7166–7182. https://doi.org/10.1002/2016JA022394

Dungey, J. W. (1956). Convective diffusion in the equatorial F region. *J. Atmos. Terr. Phys.*, *9*(5-6), 304–310. https://doi.org/10.1016/0021-9169(56)90148-9

Egedal, J. (1947). The magnetic diurnal variation of the horizontal force near the magnetic equator. *Terr. Magn. Atmos. Electr.*, *52*(4), 449–451. https://doi.org/10.1029/TE052i004p00449

Emmert, J. T., Richmond, A. D., and Drob, D. P. (2010). A computationally compact representation of magnetic-apex and quasi-dipole coordinates with smooth base vectors. *J. Geophys. Res.*, *115*(A8), A08322. https://doi.org/10.1029/2010JA015326

Farley, D. T., Balsley, B. B., woodman, R. F., and McClure, L. P. (1970). Equatorial spread F: Implications of VHF radar observations. *J. Geophys. Res.*, *75*(34), 7199–7216. https://doi.org/10.1029/JA075i034p07199

Fejer, B. G., Farley, D. T., Woodman, R. F., and Calderon, C. (1979). Dependence of equatorial F region vertical drifts on season and solar cycle. *J. Geophys. Res.*, *84*(A10), 5792–5796. https://doi.org/10.1029/JA084iA10p05792

Fejer, B. G., de Paula, E. R., Gonzáles, S. A., and Woodman, R. F. (1991). Average vertical and zonal F region plasma drifts over Jicamarca. *J. Geophys. Res.*, *96*(A8), 13901–13906. https://doi.org/10.1029/91JA01171

Fuller-Rowell, T. J., Codrescu, M. V., Moffett, R. J., and Quegan, S. (1994). Response of the thermosphere and ionosphere to geomagnetic storms. *J. Geophys. Res.*, *99*(A3), 3893–3914. https://doi.org/10.1029/93JA02015

Fukao, S., Kelley, M. C., Shirakawa, T., Takami, T., Yamamoto, M., Tsuda, T., and Kato, S. (1991). Turbulent upwelling of the mid-latitude ionosphere: 1

Observational results by the MU radar. *J. Geophys. Res.*, *96*(A3), 3725–3746. https://doi.org/10.1029/90JA02253

Graham, G. (1724-1725). An account of observations made of the variation of the horizontal needle at London, in the latter part of the year 1722, and beginning of 1723. By Mr. George Graham, Watchmaker, F. R. S. *Philos. Trans.*, 33, 96-107.

Hanson, W. B., and Moffett, R. J. (1966). Ionization transport effects in the equatorial F region. *J. Geophys. Res.*, *71*(23), 5559–5572. https://doi.org/10.1029/JZ071i023p05559

Haerendel, G. (1972). Rayleigh-Taylor instability as cause of equatorial spread-F. *Trans. Am. Geophys. Union*, *53*(11), 1082.

Hamza, A. M. (1999). Perkins instability revisited. *J. Geophys. Res.*, *104*(A10), 22567–22575. https://doi.org/10.1029/1999JA900307

Heaviside, O. (1902). *Telegraph Theory*. 10th ed. Chicago: Encyclopedia Britannica.

Hedin, A. E., Fleming, E. L., Manson, A. H., Schmidlin, F. J., Avery, S. K., Clark, R. R., Fraser, G. J., Tsuda, T., Vial, F., and Vincent, R. (1996). Empirical wind model for the upper, middle and lower atmosphere. *J. Atmos. Terr. Phys.*, *58*(3), 1421–1447. https://doi.org/10.1016/0021-9169(95)00122-0

Heelis, R. A., Kendall, P. C., Moffett, R. J., Windle, D. W., and Rishbeth, H. (1974). Electrical coupling of the E- and F-regions and its effects on F-region drifts and winds. *Planet. Space Sci.*, *22*(5), 743–756. https://doi.org/10.1016/0032-0633(74)90144-5

Huang, C. S., and Kelley, M. C. (1996). Nonlinear evolution of equatorial spread F: 2. Gravity wave seeding of Rayleigh-Taylor instability. *J. Geophys. Res.*, *101*(A1), 293–302. https://doi.org/10.1029/95JA02210

Huang, C. M., Chen, M. Q., and Liu, J. Y. (2010). Ionospheric positive storm phases at the magnetic equator close to sunset. *J. Geophys. Res.*, *115*(A7), A07315. https://doi.org/10.1029/2009JA014936

Huba, J. D., Joice, G., Sazykin, S., Wolf, R., and Spiro, R. (2005). Simulation study of penetration electric field effects on the low- to mid-latitude ionosphere. *Geophys. Res. Lett.*, *32*(23), L23101. https://doi.org/10.1029/2005GL024162

Huba, J. D., Joyce, G., and Krall, J. (2008). Three-dimensional equatorial spread F modeling. *Geophys. Res. Lett.*, *35*(10), L10102. https://doi.org/10.1029/2008GL033509

Hysell, D. L., Larsen, M. F., Swenson, C. M., Barjatya, A., Wheeler, T. F., Sarango, M. F., Woodman, R. F., and Chau, J. L. (2005). Onset conditions for equatorial spread F determined during EQUIS II. *Geophys. Res. Lett.*, *32*(24), L24104. https://doi.org/10.1029/2005GL024743

Hysell, D. L., Larsen, M. F., Swenson, C. M., and Wheeler, T. F. (2006). Shear flow effects at the onset of equatorial spread F. *J. Geophys. Res.*, *111*(A11), A11317. https://doi.org/10.1029/2006JA011963

Hysell, D. L., Jafari D. L., Milla R., Meriwether M. A., J. W. (2014). Data-driven numerical simulations of equatorial spread F in the Peruvian sector. *J. Geophys. Res. Space Phys.*, *119*, 3815–3827. https://doi.org/10.1002/2014JA019889

Jayachandran, B., Balan, N., Namboothiri, S. P., and Rao, P. B. (1987). HF Doppler observations of vertical plasma drifts in the evening F region at the equator. *J. Geophys. Res.*, *92*(A10), 11253–11256. https://doi.org/10.1029/JA092iA10p11253

Jayachandran, B., Balan, N., Rao, P. B., Sastri, J. H., and Bailey, G. J. (1993). HF Doppler and ionosonde observations on the onset conditions of equatorial spread F. *J. Geophys. Res.*, *98*(A8), 13741–13750. https://doi.org/10.1029/93JA00302

Kelley, M. C., Larsen, M. F., LaHoz, C., and McClure, J. P. (1981). Gravity wave initiation of equatorial spread F: a case study. *J. Geophys. Res.*, *86*(A11), 9087–9100. https://doi.org/10.1029/JA086iA11p09087

Kelley, M. C., and Fukao, S. (1991). Turbulent upwelling of the mid-latitude ionosphere, II: theoretical framework. *J. Geophys. Res.*, *96*, 3747–3753.

Kelley, M. C., Vlasov, M. N., Foster, J. C., and Coster, A. J. (2004). A quantitative explanation for the phenomenon known as storm-enhanced density. *Geophys. Res. Lett.*, *31*(19), L19809. https://doi.org/10.1029/2004GL020875

Kelley, M. C., Makela, J. J., de La Beaujardière, O., and Retterer, J. (2011). Convective ionospheric storms: a review. *Rev. Geophys.*, *49*(2), RG2003. https://doi.org/10.1029/2010RG000340

Kelley, M. C., and Dao, E. V. (2017). Evidence for gravity wave seeding of convective ionospheric storms possibly initiated by thunderstorms. *J. Geophys. Res. Space Phys.*, *122*(5), 4046–4052. https://doi.org/10.1002/2017JA024707

Kennelly, A. E. (1902). On the elevation of the electrically-conducting strata of the Earth's atmosphere. *Electr. World Engineer*, *39*, 473.

Kikuchi, T., Araki, T., Maeda, H., and Maekawa, K. (1978). Transmission of polar electric fields to the equator. *Nature*, *273*(5664), 650–651. https://doi.org/10.1038/273650a0

Kudeki, E., and Bhattacharyya, S. (1999). Postsunset vortex in equatorial F-region plasma drifts and implications for bottomside spread-F. *J. Geophys. Res.*, *104*(A12), 28163–28170. https://doi.org/10.1029/1998JA900111

Kudeki, E., Akgiray, A., Milla, M. A., Chau, J. L., and Hysell, D. L. (2007). Equatorial spread-F initiation: post-sunset vortex, thermospheric winds, gravity waves. *J. Atmos. Solar Terr. Phys.*, *69*(17-18), 2416–2427. https://doi.org/10.1016/j.jastp.2007.04.012

Li, G. Z., Ning, B. Q., and Yuan, H. (2007). Analysis of ionospheric scintillation spectra and TEC in the Chinese low latitude region. *Earth Planet. Space*, *59*(4), 279–285. https://doi.org/10.1186/BF03353105

Lin, C. H., Richmond, A. D., Heelis, R. A., Bailey, G. J., Lu, G., Liu, J. Y., Yeh, H. C., and Su, S. Y. (2005). Theoretical study of the low- and midlatitude ionospheric electron density enhancement during the October 2003 superstorm: Relative importance of the neutral wind and the electric field. *J. Geophys. Res.*, *110*(A12), A12312. https://doi.org/10.1029/2005JA011304

Liu, H., and Lühr, H. (2005). Strong disturbance of the upper thermospheric density due to magnetic storms: CHAMP observations. *J. Geophys. Res.*, *110*(A9), A09S29. https://doi.org/10.1029/2004JA010908

Liu, L. B., He, M. S., Yue, X. A., Ning, B. Q., and Wan, W. X. (2010). Ionosphere around equinoxes during low solar activity. *J. Geophys. Res.*, *115*(A9), A09307. https://doi.org/10.1029/2010JA015318

Lu, G., Goncharenko, L. P., Nicolls, M. J., Maute, A. I., Coster, A. J., and Paxton, L. J. (2012). Ionospheric and thermospheric variations associated with prompt penetration electric fields. *J. Geophys. Res.*, *117*(A8), A08312. https://doi.org/10.1029/2012JA017769

Madhav Haridas, M. K., Manju, G., and Pant, T. K. (2013). First observational evidence of the modulation of the threshold height h'Fc for the occurrence of equatorial spread F by neutral composition changes. *J. Geophys. Res. Space Phys.*, *118*(6), 3540–3545. https://doi.org/10.1002/jgra.50331

Makela, J. J., and Otsuka, Y. (2012). Overview of nighttime ionospheric instabilities at low- and mid-latitudes: coupling aspects resulting in structuring at the mesoscale. *Space Sci. Rev.*, *168*(1-4), 419–440. https://doi.org/10.1007/s11214-011-9816-6

Mannucci, A. J., Tsurutani, B. T., Iijima, B. A., Komjathy, A., Saito, A., Gonzalez, W. D., Guarnieri, F. L., Kozyra, J. U., and Skoug, R. (2005). Dayside global ionospheric response to the major interplanetary events of October 29-30, 2003 "Halloween Storms". *Geophys. Res. Lett.*, *32*(12), L12S02. https://doi.org/10.1029/2004GL021467

Maruyama, T. (1990). E×B instability in the F-region at low-to midlatitudes. *Planet. Space Sci.*, *38*(2), 273–285. https://doi.org/10.1016/0032-0633(90)90092-5

Martyn, D. F. (1955). Theory of height and ionization density changes at the maximum of a Chapman-like region, taking account of ion production, decay, diffusion, and total drift. In *Proceedings, Cambridge Conference* (pp. 254). London: Physical Society.

Mitra, S. K. (1946). Geomagnetic control of region F2 of the ionosphere. *Nature*, *158*(4019), 668–669. https://doi.org/10.1038/158668a0

Moffett, R. J. (1979). The equatorial anomaly in the electron distribution of the terrestrial F-region. *Fund. Cosmic Phys.*, *4*, 313.

Moffett, R. J., and Hanson, W. B. (1965). Effect of ionization transport on the equatorial F-region. *Nature*, *206*(4985), 705–706. https://doi.org/10.1038/206705a0

Namba, S., and Maeda, K. I. (1939). *Radio Wave Propagation*. Tokyo: Corona.

Namboothiri, S. P., Balan, N., and Rao, P. B. (1989). Vertical plasma drifts in the F region at the magnetic equator. *J. Geophys. Res.*, *94*(A9), 12055–12060. https://doi.org/10.1029/JA094iA09p12055

Narayanan, V. L., Shiokawa, K., Otsuka, Y., and Saito, S. (2014). Airglow observations of nighttime medium-scale traveling ionospheric disturbances from Yonaguni: Statistical characteristics and low-latitude limit. *J. Geophys. Res.*, *119*(11), 9268–9282. https://doi.org/10.1002/2014JA020368

Oyama, K. I., Abdu, M. A., Balan, N., Bailey, G. J., Watanabe, S., Takahashi, T., de Paula, E. R., Batista, I. S., Isoda, F., and Oya, H. (1997). High electron temperature associated with the prereversal enhancement in the equatorial ionosphere. *J. Geophys. Res.*, *102*(A1), 417–424. https://doi.org/10.1029/96JA02705

Otsuka, Y., Shiokawa, K., Ogawa, T., and Wilkinson, P. (2002). Geomagnetic conjugate observations of equatorial airglow depletions. *Geohys. Res. Let.*, *29*(15), 43–1. https://doi.org/10.1029/2002GL015347

Otsuka, Y., Shiokawa, K., Nishioka, M., and Effendy, V. (2012). VHF radar observations of post-midnight F-region field-aligned irregularities over Indonesia during solar minimum. *Indian J. Radio Space Phys.*, *41*(2), 199–207.

Patra, A. K., Taori, A., Chaitanya, P. P., and Sripathi, S. (2013). Direct detection of wavelike spatial structure at the bottom of the F region and its role on the formation of equatorial plasma bubble. *J. Geophys. Res.*, *118*(3), 1196–1202. https://doi.org/10.1002/jgra.50148

Perkins, F. (1973). Spread F and ionospheric currents. *J. Geophys. Res.*, *78*(1), 218–226. https://doi.org/10.1029/JA078i001p00218

Picone, J. M., Hedin, A. E., Drob, D., and Aikin, A. C. (2002). NRLMSISE-00 empirical model of the atmosphere: statistical comparisons and scientific issues. *J. Geophys. Res.*, *107*(A12), 1468. https://doi.org/10.1029/2002JA009430

Prakash, S. (1999). Production of electric field perturbations by gravity wave winds in the E region suitable for initiating equatorial spread F. *J. Geophys. Res.*, *104*(A5), 10051–10069. https://doi.org/10.1029/1999JA900028

Prolss, G. W. (1995). Ionospheric F-region storms. In H. Volland (Ed.), *Handbook of Atmospheric Electrodynamics* (pp. 195–245). Boca Raton: CRC Press.

Raghavarao, R., Wharton, L. E., Spencer, N. W., Mayr, H. G., and Brace, L. H. (1991). An equatorial temperature and wind anomaly (ETWA). *Geophys. Res. Letts.*, *18*(7), 1193–1196. https://doi.org/10.1029/91GL01561

Rajaram, G. (1977). Structure of the equatorial F-region, topside and bottomside - A review. *J. Atmos. Terr. Phys.*, *39*(9-10), 1125–1144. https://doi.org/10.1016/0021-9169(77)90021-6

Ratcliffe, J. A. (1972). *Introduction to the Ionosphere and Magnetosphere*. Cambridge: Cambridge University Press.

Rastogi, R. G. (1977). Geomagnetic storms and electric fields in the equatorial ionosphere. *Nature*, *268*(5619), 422–424. https://doi.org/10.1038/268422a0

Rastogi, R. G., Mullen, J. P., and MacKenzie, E. (1981). Effect of geomagnetic activity on equatorial radio VHF scintillations and spread F. *J. Geophys. Res.*, *86*(A5), 3661–3664. https://doi.org/10.1029/JA086iA05p03661

Rishbeth, H., Lyon, A. J., and Peart, M. (1963). Diffusion in the equatorial F layer. *J. Geophys. Res.*, *68*(9), 2559–2569. https://doi.org/10.1029/JZ068i009p02559

Rishbeth, H. (1971). The F-layer dynamo. *Planet. Space Sci.*, *19*(2), 263–267. https://doi.org/10.1016/0032-0633(71)90205-4

Sahai, Y., Becker-Guedes, F., Fagundes, P. R., de Abreu, A. J., de Jesus, R., Pillat, V. G., Abalde, J. R., Martinis, C. R., Brunini, C., … Otsuka Y. (2009). Observations of the F-region ionospheric irregularities in the South American sector during the October 2003 "Halloween Storms". *Ann. Geophys.*, *27*(12), 4463–4477. https://doi.org/10.5194/angeo-27-4463-2009

Scannapieco, A. J., and Ossakow, S. L. (1976). Nonlinear equatorial spread F. *Geophys. Res. Lett.*, *3*(8), 451–454. https://doi.org/10.1029/GL003i008p00451

Sekar, R., Suhasini, R., and Raghavarao, R. (1995). Evolution of plasma bubbles in the equatorial F region with different seeding conditions. *Geophys. Res. Lett.*, *22*(8), 885–888. https://doi.org/10.1029/95GL00813

Shiokawa, K., Otsuka, Y., Ejiri, M. K., Sahai, Y., Kadota, T., Ihara, C., Ogawa, T., Igarashi, K., Miyazaki, S., and Saito, A. (2002). Imaging observations of the equatorward limit of midlatitude traveling ionospheric disturbances. *Earth Planet. Space*, *54*(1), 57–62. https://doi.org/10.1186/BF03352421

Souza, J. R., Asevedo Jr, W. D., dos Santos, P. C. P., Petry, A., Bailey, G. J., Batista, I. S., and Abdu, M. A. (2013). Longitudinal variation of the equatorial ionosphere: Modeling and experimental results. *Adv. Space Res.*, *51*(4), 654–660. https://doi.org/10.1016/j.asr.2012.01.023

Sreeja, V., Ravindran, S., Pant, T. K., Devasia, C. V., and Paxton, L. J. (2009). Equatorial and low-latitude ionosphere-thermosphere system response to the space weather event of August 2005. *J. Geophys. Res.*, *114*(A12), A12307. https://doi.org/10.1029/2009JA014491

Stening, R. J. (1992). Modelling the low latitude F region. *J. Atmos. Terr. Phys.*, *54*(11-12), 1387–1412. https://doi.org/10.1016/0021-9169(92)90147-D

Stolle, C., Michaelis, I., and Rauberg, J. (2016). The role of high-resolution geomagnetic field models for investigating ionospheric currents at low Earth orbit satellites. *Earth Planet. Space*, *68*, 110. https://doi.org/10.1186/s40623-016-0494-1

Su, S. Y., Liu, C. H., Ho, H. H., and Chao, C. K. (2006). Distribution characteristics of topside ionospheric density irregularities: equatorial versus midlatitude regions. *J. Geophys. Res.*, *111*(A6), A06305. https://doi.org/10.1029/2005JA011330

Sultan, P. J. (1996). Linear theory and modeling of the Rayleigh–Taylor instability leading to the occurrence of equatorial spread F. *J. Geophys. Res.*, *101*(A12), 26875–26891. https://doi.org/10.1029/96JA00682

Taylor, J. E. (1902-1903). Characteristics of electric earth-current disturbances, and their origin. *Proc. R. Soc. London*, *71*, 225–227.

Thampi, S. V., Ravindran, E., Pant, T. K., Devasia, C. V., Sreelatha, P., and Sridharan, R. (2006). Deterministic prediction of post-sunset ESF based on the strength and asymmetry of EIA from ground based TEC measurements: Preliminary results. *Geophys. Res. Lett.*, *33*(13), L13103. https://doi.org/10.1029/2006GL026376

Tsunoda, R. T. (1985). Control of the seasonal and longitudinal occurrence of equatorial scintillations by the longitudinal gradient in integrated E region Pedersen conductivity. *J. Geophys. Res.*, *90*, 447–456.

Tsunoda, R. T. (2006). On the coupling of layer instabilities in the nighttime midlatitude ionosphere. *J. Geophys. Res.*, *111*(A11), A11304. https://doi.org/10.1029/2006JA011630

Tsunoda, R. T., and Cosgrove, R. B. (2001). Coupled electrodynamics in the nighttime midlatitude ionosphere. *Geophys. Res. Lett.*, *28*(22), 4171–4174. https://doi.org/10.1029/2001GL013245

Tsunoda, R. T., Bubenik, D. M., Thampi, S. V., and Yamamoto, M. (2010). On large-scale wave structure and equatorial spread F without a post-sunset rise of the F layer. *Geophys. Res. Lett.*, *37*(7), L07105. https://doi.org/10.1029/2009GL042357

Tulasi Ram, S., Rama Rao, P. V. S., Prasad, D. S. V. V. D., Niranjan, K., Gopi Krishna, S., Sridharan, R., and Ravindran, S. (2008). Local time dependant response of postsunset ESF during geomagnetic storms. *J. Geophys. Res.*, *113*(A7), A07310. https://doi.org/10.1029/2007JA012922

Tulasi Ram, S., Yamamoto, M., Tsunoda, R. T., Chau, H. D., Hoang, T. L., Damtie, B., Wassaie, M., Yatini, C. Y., Manik, T., and Tsugawa, T. (2014). Characteristics of large-scale wave structure observed from African and Southeast Asian longitudinal sectors. *J. Geophys. Res.*, *119*(3), 2288–2297. https://doi.org/10.1002/2013JA019712

Viggiano, A. A., and Arnold, F. (1995). Ion chemistry and composition of the atmosphere. In H. Volland (Ed.), *Handbook of Atmospheric Electrodynamics*. Boca Raton: CRC Press.

Whalen, J. A. (2002). Dependence of equatorial bubbles and bottomside spread F on season, magnetic activity, and **E**×**B** drift velocity during solar maximum. *J. Geophys. Res.*, *107*(A2), SIA 3-1–SIA 3-9. https://doi.org/10.1029/2001JA000039

Woodman, R. F., and La Hoz, C. (1976). Radar observations of F region equatorial irregularities. *J. Geophys. Res.*, *81*(31), 5447–5466. https://doi.org/10.1029/JA081i031p05447

Woodman, R. F. (2009). Spread F—an old equatorial aeronomy problem finally resolved?. *Ann. Geophys.*, *27*(5), 1915–1934. https://doi.org/10.5194/angeo-27-1915-2009

Weber, E. J., Buchau, J., Eather, R. H., and Mende, S. B. (1978). North-south aligned equatorial airglow depletions. *J. Geophys. Res.*, *83*(A2), 712–716. https://doi.org/10.1029/JA083iA02p00712

Yokoyama, T., Shinagawa, H., and Jin, H. (2014). Nonlinear growth, bifurcation, and pinching of equatorial plasma bubble simulated by three-dimensional high-resolution bubble model. *J. Geophys. Res. Space Phys.*, *119*(12), 10474–10482. https://doi.org/10.1002/2014JA020708

Yokoyama, T., and Stolle, C. (2017). Low and midlatitude ionospheric plasma density irregularities and their effects on geomagnetic field. *Space Sci. Rev.*, *206*(1-4), 495–519. https://doi.org/10.1007/s11214-016-0295-7

Zalesak, S. T., Ossakow, S. L., and Chaturvedi, P. K. (1982). Nonlinear equatorial spread F: the effect of neutral winds and background Pedersen conductivity. *J. Geophys. Res.*, *87*(A1), 151–166. https://doi.org/10.1029/JA087iA01p00151